

## Early diagenetic cycling, incineration, and burial of sedimentary organic carbon in the central Gulf of Papua (Papua New Guinea)

Robert C. Aller,<sup>1</sup> Neal E. Blair,<sup>2,3</sup> and Gregg J. Brunskill<sup>4</sup>

Received 15 September 2006; revised 23 March 2007; accepted 31 May 2007; published 12 January 2008.

[1] The clinoform complex of the Gulf of Papua represents a major deltaic system in Oceania. Two seasons largely control seafloor dynamics and sedimentary C cycling: the relatively quiescent NW monsoon, and the SE trades, characterized by remobilization and reoxidation of topset deposits. Surface sediments (~20 cm) are reactive with  $\Sigma\text{CO}_2$  production fluxes  $\sim 35\text{--}42 \text{ mmol m}^{-2} \text{ d}^{-1}$  at mangrove channel and topset sites during the monsoon, and  $\sim 10\text{--}20 \text{ mmol m}^{-2} \text{ d}^{-1}$  on the foreset-bottomset (>40 m).

Fluxes decrease by a factor of  $\sim 0.3$  on the topset during the transition period and trades. The  $^{13,14}\text{C}$  isotopic compositions of pore water  $\Sigma\text{CO}_2$  reveal diagenetic fractionation, with dominant utilization of young ( $\Delta^{14}\text{C} = 1.4\text{--}31.1\text{\textperthousand}$ ), terrestrial C substrates inshore (channels, topset  $\delta^{13}\text{C} = -29$  to  $-25\text{\textperthousand}$ ) and a progressive increase of young marine C sources seaward (outer topset, foreset; bottomset  $\delta^{13}\text{C} = -22.2$  to  $-19.5$ ). Remineralization patterns of terrestrial and marine  $\text{C}_{\text{org}}$  demonstrate cross-shelf exchange. Multiple tracers show that a suboxic, mobile mud layer,  $\sim 10\text{--}60 \text{ cm}$  thick (usually  $\sim 10\text{--}30 \text{ cm}$ ), characterizes the central gulf topset and Umuda Valley off the Fly River and unconformably overlies methanic deposits releasing old  $\Sigma\text{CO}_2$  ( $\Delta^{14}\text{C} = -159$  to  $-229\text{\textperthousand}$ ). Residual terrestrial  $\text{C}_{\text{org}}$  delivered to the bioturbated foreset continues to be remineralized slowly, generating  $\Sigma\text{CO}_2$  having net  $\Delta^{14}\text{C} = -270$  within sediments deposited 100–200 years ago. The reactivity of  $\text{C}_{\text{org}}$  below  $\sim 0.5 \text{ m}$  in the foreset is  $\sim 10\text{--}20$  times lower than expected based on accumulation rates, reflecting loss of >50% of sedimentary  $\text{C}_{\text{org}}$  on the topset, which functions as a suboxic incinerator.

**Citation:** Aller, R. C., N. E. Blair, and G. J. Brunskill (2008), Early diagenetic cycling, incineration, and burial of sedimentary organic carbon in the central Gulf of Papua (Papua New Guinea), *J. Geophys. Res.*, 113, F01S09, doi:10.1029/2006JF000689.

### 1. Introduction

[2] Deltaic systems are widely recognized as the major storage sites for inorganic sedimentary debris and organic carbon along continental boundaries [Berner, 1982; Hedges and Keil, 1995; Burdige, 2007]. They are also regions of elevated primary production, intense biogeochemical cycling, and dynamic refluxing of material between multiple depositional and diagenetic facies. Understanding the processing, addition, alteration, and burial of riverine, wetland, and marine derived material within these complex sedimentary ecosystems remains a central goal of coastal ocean biogeochemistry [Benner, 2004; McKee et al., 2004; Blair et al., 2004; Goñi et al., 2005]. Tropical deltas are of particular

interest because the tropics supply  $\sim 60 \pm 10\%$  of the global river water and sediment delivery to coastal lowlands and the ocean, and a comparable percentage of the riverine particulate and dissolved organic carbon flux [Milliman and Meade, 1983; Alongi, 1998; Meybeck, 1993; Ludwig et al., 1996; Schlünz and Schneider, 2000; Jennerjahn and Ittekkot, 2002]. Because of numerous mountainous rivers with high drainage basin yield, tectonically active Oceania accounts for roughly half of the tropical zone fluxes, with the island of New Guinea alone supplying as much as  $1.5 \times$  the amount of sediment and organic C ( $\text{C}_{\text{org}}$ ) derived from the much larger Amazon basin [Milliman, 1995; Milliman et al., 1999; Bird et al., 1995; Lyons et al., 2002].

[3] One of the major deltaic systems in Oceania is located in the Gulf of Papua, a semicircular embayment of the continental shelf on the south coast of Papua New Guinea (Figure 1). The coalescence of the Fly, Bamu, Turama, Kikori, and Purari rivers along the northern boundary of the gulf results in a broad swath of mangrove forests and the progradation of deltaic deposits into energetic coastal waters of the Coral Sea [Harris et al., 1993, 1996; Robertson et al., 1998; Walsh and Nittrouer, 2004; Walsh et al., 2004]. The Gulf of Papua system thus combines high-yield mountainous river source regions, which are typical of tectonically

<sup>1</sup>School of Marine and Atmospheric Sciences, State University of New York at Stony Brook, Stony Brook, New York, USA.

<sup>2</sup>Department of Marine, Earth, and Atmospheric Sciences, North Carolina State University, Raleigh, North Carolina, USA.

<sup>3</sup>Now at Department of Civil and Environmental Engineering, Department of Earth and Planetary Sciences, Northwestern University, Evanston, Illinois, USA.

<sup>4</sup>Australian Institute of Marine Science, Townsville, Queensland, Australia.

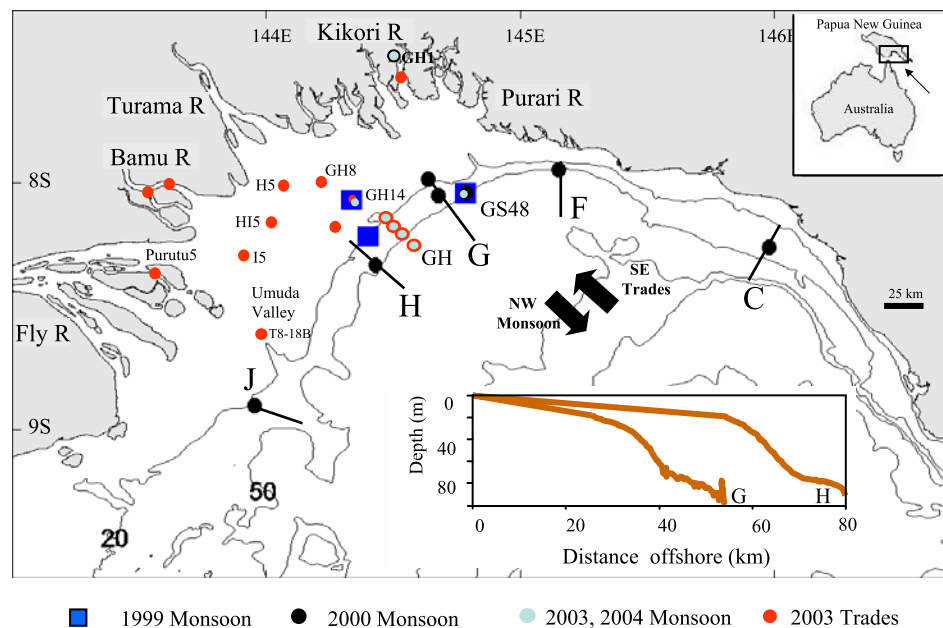


**Figure 1.** Locations are plotted of stations sampled seasonally in the Gulf of Papua during the monsoon through trades seasons 2003–2004 and during previous studies in 1997–2000 at the same or nearby sites. The primary study transect, GH, lies between transects G and H which were established in 2000, along with transects C → J, and sampled from the R/V *Franklin*. Stations indicated by HM (squares) were sampled from the R/V *Harry Messel* during 1999, sites HM50 and HM13 of which are comparable to GS48 and GH14 of the present study [Aller et al., 2004; Aller and Blair, 2004]. The bottom right inset shows inshore-offshore bathymetric profiles along G and H, extrapolated to the shoreline, illustrating the prograding clinoform character of the system [Walsh et al., 2004]. Primary wind directions during the NW monsoon and SE trades periods are indicated. The top right inset shows the location of the Gulf of Papua relative to the island of New Guinea and Australia.

active margins known to supply a high proportion of refractory  $C_{org}$  to the ocean, with a broad shelf and energetic deltaic depocenter, which are often associated with passive margins and the efficient diagenetic remineralization of sedimentary  $C_{org}$  [Blair et al., 2004; Komada et al., 2004; Leithold et al., 2006; Aller and Blair, 2006]. This union of conditions has unusual potential to provide new insights into the factors controlling the cycling and burial of both old refractory and recent labile sedimentary  $C_{org}$  in the coastal ocean.

[4] In the present study, we substantially extend previous quantitative investigations of the relationship between depositional environment, early diagenetic cycling, and preservation of  $C_{org}$  in the central Gulf of Papua clinoform delta. Our primary purposes are to constrain further the overall patterns of remineralization and net burial of terrestrial and marine  $C_{org}$  in the subaqueous deposits, to examine seasonal variability, to refine conceptual models of the primary factors controlling these patterns, and to construct facies-specific sedimentary  $C_{org}$  cycling budgets. In addition to direct measurements of remineralization rates and  $C_{org}$  fluxes, we utilize extensive new data on  $^{13}C/^{12}C$  and  $^{14}C/^{12}C$  isotopic distributions of pore water  $\Sigma CO_2$  and solid  $C_{org}$ , and diagenetic modeling to infer source, reactivity, and fate of sedimentary  $C_{org}$  in the different major facies of the deltaic complex. It is demonstrated that a wide spectrum of terrestrial soil, mangrove (vascular plant), and marine planktonic  $C_{org}$  debris introduced to the central gulf is

remineralized on the shallow clinoform topset and within active channels, apparently as a consequence of sediment refluxing coupled with oxic/suboxic diagenesis. Although both terrestrial and marine-derived  $C_{org}$  substrates are decomposed throughout the clinoform, there is a progressive increase of marine substrate utilization offshore, accounting for nearly 100% of remineralization in the bottomset (75 m). Diagenetic fractionation of  $C_{org}$  substrates during remineralization is the general rule with preferential loss of young relative to old  $C_{org}$ ; however, slow remineralization of aged  $C_{org}$  (>2000 years) is evident throughout the central gulf, and a wide range of labile and refractory  $C_{org}$  (>modern to >4800 years) can be decomposed within migrating mangrove channel deposits. The residual sedimentary  $C_{org}$  escaping seaward from the dynamic, shallow water incineration zone is relatively refractory. As a result, bulk  $C_{org}$  supports lower rates of decomposition in the delta foreset than might otherwise be expected based on the rapid accumulation rates that occur there and on previously established correlations between  $C_{org}$  reactivity and sediment accumulation in nondeltaic environments.

## 2. Study Area

[5] The rivers entering the Gulf of Papua are estimated to deliver  $\sim 384 \text{ Mt a}^{-1}$  of sediment and  $470\text{--}690 \text{ km}^3$  fluid per years into lowland and coastal areas ( $\text{Mt} = 10^6 \text{ t}$ )

[Milliman et al., 1999; Pickup and Chewings, 1983; Salomons and Eagle, 1990; Wolanski et al., 1995]. The Fly is the largest of these rivers and supplies  $\sim 85\text{--}115 \text{ Mt a}^{-1}$  and  $190\text{--}220 \text{ km}^3 \text{ fluid a}^{-1}$ . These sediment/water delivery ratios ( $\text{Mt km}^{-3}$ ) are about  $4\text{--}10\times$  higher than other major tropical rivers such as the Amazon and Congo, reflecting the high-relief drainage basin [Milliman and Meade, 1983; Milliman and Syvitski, 1992]. Although river runoff is relatively constant seasonally, major interannual decreases occur during El Niño drought conditions [Pickup and Chewings, 1983; Wolanski et al., 1984, 1995; Moi, 2001; Walsh et al., 2004]. Such climatic events may significantly affect sediment storage and delivery patterns [Ogston et al., 2008]. The quantity of sediment actually making it into the estuarine zones and seaward is uncertain and may be substantially lower than the estimated drainage basin yields and gauged transport, likely averaging  $\sim 156 \text{ Mt a}^{-1}$  over decadal timescales [Brunskill et al., 2007a, 2007b]. This latter estimate of the realized sediment supply to the gulf is consistent with sediment accumulation budgets in the mangrove forests, delta plain, and shelf, which can account for  $\sim 138 \text{ Mt a}^{-1}$  [Walsh et al., 2004; Walsh and Nittrouer, 2004; Brunskill et al., 2003, 2007a, 2007b].

[6] The shelf extends up to  $\sim 150 \text{ km}$  in the central gulf, narrowing eastward toward Kerema and westward into the Torres Strait, both of which are regions characterized by coral reefs. Most sediment accumulates on the inner shelf of the central gulf in  $<50 \text{ m}$  of water as part of an overall prograding clinoform deposit [Harris et al., 1996; Walsh et al., 2004]; however, off the Fly, a portion moves seaward within incised relict river channels such as the subaqueous Umuda Valley [Martin et al., 2008]. Approximately 65% of the sediment flux accumulates in 30% of the inner shelf area between  $\sim 30$  and  $50 \text{ m}$  depth within the clinoform foreset. Net accumulation rates on the foreset are  $\sim 1\text{--}4 \text{ cm a}^{-1}$  ( $1\text{--}3.8 \text{ g cm}^{-2} \text{ a}^{-1}$ ). Roughly 25% of the flux accumulates in the broad, low-gradient topset between 0 and  $20 \text{ m}$ , representing nearly 70% of the inner shelf area [Brunskill et al., 2003; Walsh et al., 2004]. The upper  $10\text{--}100 \text{ cm}$  of silty mud deposits in the topset are highly reworked and mobile (usually  $10\text{--}30 \text{ cm}$ ), making estimates of accumulation in this zone uncertain. Mangrove forest accretion apparently accounts for  $\sim 5\text{--}10\%$  of the sediment flux [Walsh and Nittrouer, 2004]. The seabed becomes progressively more carbonate rich with sands and local hard grounds seaward of the bottomset zone at depths  $>75\text{--}100 \text{ m}$  [Brunskill et al., 1995; Harris et al., 1996]. Only a small fraction of river sediment input,  $<5\%$ , is believed to be exported off shelf into the Pandora Trough [Brunskill et al., 2003; Walsh and Nittrouer, 2003; Muhammad et al., 2008].

[7] The river mouths and proximal delta regions are characterized by migrating sandy estuarine channels, mud banks, and highly productive mangrove forests [Harris et al., 1993, 1996; Alongi et al., 1992; Robertson et al., 1998; Walsh and Nittrouer, 2004]. Before entering these coastal areas, riverbed and suspended matter particulate organic carbon (POC) typically ranges from  $\sim 900$  to  $1200 \mu\text{mol C}_{\text{org}} \text{ g}^{-1}$ , solid C/N  $\sim 13$  to  $15 (\text{mol mol}^{-1})$ , and dissolved organic carbon (DOC)  $\sim 250 \mu\text{M}$ . [Bird et al., 1994, 1995; Salomons and Eagle, 1990; Robertson et al., 1998; Goñi et al., 2006]. Net addition of mangrove forest detritus and

planktonic production within the estuarine and delta plain zones locally augments suspended particulate  $\text{C}_{\text{org}}$  to levels exceeding  $8000 \mu\text{mol C g}^{-1}$ , elevates C/N to  $\sim 20\text{--}45$ , and depletes DOC by  $\sim 30\%$  [Robertson et al., 1998; Goñi et al., 2006]. In contrast, sedimentary  $\text{C}_{\text{org}}$  accumulating in seaward deposits on the topset and foreset ranges between  $\sim 200$  and  $1200 \mu\text{mol C}_{\text{org}} \text{ g}^{-1}$  with typical C/N  $\sim 7\text{--}15$  [Brunskill et al., 1995, 1996; Bird et al., 1995; Goñi et al., 2006]. The lowest  $\text{C}_{\text{org}}$  and highest C/N occur off the southern channel of the Fly, associated with relatively coarse deposits. Low  $\text{C}_{\text{org}}$  concentrations are also found in carbonate deposits and hard grounds offshore. Bulk  $\text{C}_{\text{org}}$  isotope distributions in surface sediment show regular inshore–offshore changes in the central gulf from predominantly terrestrially derived  $\text{C}_{\text{org}}$  ( $\delta^{13}\text{C} = -26.5 \pm 0.5\%$ ) over much of the inner topset to dominantly marine planktonic sources in the deeper foreset and bottomset ( $\delta^{13}\text{C} = -20.5 \pm 0.5\%$ ) [Bird et al., 1995; Aller and Blair, 2004; Goñi et al., 2006]. The average  $^{14}\text{C}$  age of bulk sedimentary  $\text{C}_{\text{org}}$  in the upper  $0\text{--}3 \text{ m}$  on the topset and foreset ranges between  $\sim 5750$  years in the western gulf and as young as 300 years in surface sediment in the east, however, most ages are  $>2000$  years, reflecting the input of either recycled sedimentary rock  $\text{C}_{\text{org}}$  (kerogen) or aged soil  $\text{C}_{\text{org}}$  [Aller and Blair, 2004; Goñi et al., 2006].

[8] Balances between tidal currents, estuarine flow, seasonal wind wave forcing, a large-scale clockwise gyre, and local geomorphologic features determine sediment accumulation patterns and transport dynamics in the gulf. Tidal range decreases from macrotidal in the west, reaching up to  $\sim 5 \text{ m}$  in the mouth of the Fly, to mesotidal off the Purari [Wolanski and Eagle, 1991; Thom and Wright, 1983]. This regular variation in range is reflected in the progressive dominance of funnel-shaped river mouth morphologies in the west [Dalrymple et al., 2003]. Tide- and wave-generated fluid muds and resuspended sediment move in and out of the coastal channels, extensively refluxing and exchanging sediment with inner shelf deposits, and complicating estimates of net sediment flux [Wolanski et al., 1995; Harris et al., 2004]. Wind wave forcing and associated disturbance of the seabed change seasonally. During the NW monsoon period (January to March) winds average  $2\text{--}5 \text{ m s}^{-1}$  with typical wave heights of  $\sim 0.3 \text{ m}$ , whereas during the SE trades period (May to October) winds average  $5\text{--}8 \text{ m s}^{-1}$ , with maximum sustained wind typically  $10\text{--}12 \text{ m s}^{-1}$  (gusts  $>20$ ), and average wave heights  $\sim 1.3 \text{ m}$  (with individual sets  $>3 \text{ m}$  on the topset, based on our direct observations) [McAlpine et al., 1983; Thom and Wright, 1983; <http://www.ncdc.noaa.gov>]. Resuspension on the topset and the generation of fluid muds during the SE trades, and subsequent pulsed export to the foreset are believed to be a primary means of clinoform progradation [Walsh et al., 2004].

[9] The shelf water column is warm ( $\sim 28 \pm 2^\circ\text{C}$ ), well oxygenated, and bottom sediments diagenetically reactive, with diffusive uptake of  $\text{O}_2$  by bottom deposits averaging  $\sim 23 \pm 15 \text{ mmol m}^{-2} \text{ d}^{-1}$  [Mitchell, 1982; Alongi et al., 1992; Alongi, 1995; Aller et al., 2004]. Benthic biological and diagenetic properties are closely tied to sediment dynamics and depositional facies. Despite high remineralization and net sediment accumulation rates, topset and upper foreset deposits are typically suboxic, dominated by

**Table 1.** Core Station Locations<sup>a</sup>

Station	Cruise	Date	Latitude °S	Longitude °E	Depth, m	Site
GH1	CF0301 monsoon	19 Feb 2003	7.483	144.506	1–3	Wame River, Aird-Purari delta
GH8	CF0302 trades	9 Nov 2003	8.001	144.229	8	inner topset
GH14	CF0301 monsoon	12 Feb 2003	8.079	144.336	14–15	topset
GH14	CF0302	11 Nov 2003				
GH14	MV0104 monsoon	18 Jan 2004				
GH14	MV0404 transition	12 May 2004				
GH25	CF0301	14 Feb 2003	8.147	144.477		topset
GH25	MV0404	18 Sept 2003			25	
GH35	CF0301	20 Feb 2003	8.181	144.505	35	outer topset-foreset
GH35	MV0404	10 May 2004				
GH50	CF0301	16 Feb 2003	8.213	144.541	50	foreset
GH50	MV0803 trades	21,25 Sep 2003				
GH75	CF0301	22 Feb 2003	8.255	144.585	75	bottomset
GS48	CF0301	24 Feb 2003	8.037	144.794	48	foreset
GS48	MV0104	14 Jan 2004				
Pai'a10	CF0302	7 Nov 2003	7.567	144.535	10	Pai'a Inlet, Aird-Purari delta
Bamu2	CF0302	13 Nov 2003	7.998	143.605	2	Bamu River channel
Bamu10	CF0302	14 Nov 2003	7.997	143.631	8	Bamu River channel
Purutu5	CF0302	16 Nov 2003	8.381	143.573	3	Purutu Island channel
H5	CF0302	10 Nov 2003	8.013	144.069	5	inner topset
H14	CF0302	18 Nov 2003	8.180	144.300	14	topset
HI5	CF0302	17 Nov 2003	8.302	143.921	6	topset
I5	CF0302	15 Nov 2003	8.346	143.880	6	inner topset
T8-18	MV0803	23 Sep 2003	8.6153	143.9755	18	Umuda Valley
T8-18	MV0104	21 Jan 2004				
T8-18	MV0404	8 May 2004				

<sup>a</sup>Additional latitude-longitude of individual core sites of Aller et al. [2008].

Fe, Mn reduction, and nonsulfidic over 0.1–1 m depth intervals [Alongi, 1995; Aller et al., 2004]. Because of physical reworking, large areas of the topset region (<20 m depth) are characterized by relatively depauperate macrobenthic communities and are dominated by microbial biomass [Alongi and Robertson, 1995; Aller and Aller, 2004; Aller et al., 2008]. Macrofaunal activity increases substantially at depths >30 m and at locally protected sites inshore, as expressed by both increasing biomass and the progressive occurrence of biogenic sedimentary structures.

### 3. Sampling

[10] Five sampling campaigns spanning the NW monsoon and SE trades periods were carried out from February 2003 to May 2004. The R/V *Cape Ferguson* (Australian Institute of Marine Science) was used for both shallow water (<15 m) and offshore sampling in February 2003 (monsoon) and November 2003 (end of trades). The R/V *Melville* (Scripps Institution of Oceanography) was used during August–September 2003 (trades), January 2004 (monsoon), and May 2004 (monsoon → trades transition) at sites deeper than ~15 m. A primary inshore–offshore transect, GH, was established in the central gulf and augmented by additional sites on the foreset (GS48), topset, mangrove and estuarine channels, and the incised Umuda Valley off the northern entrance of the Fly (Table 1 and Figure 1) (see Aller et al. [2008] for a more complete location listing). The GH transect and station GS48 were close to or overlapped with sites sampled during previous studies in 1997–2000 on the R/V *Franklin* and R/V *Harry Messel* [Walsh et al., 2004; Aller et al., 2004; Aller and Blair, 2004], and were designed to seasonally sample the shallow topset and deeper foreset facies of the clinoform. The number

accompanying station designations indicates approximate water depth (e.g., GH50 = 50 m depth).

#### 3.1. Overlying Water

[11] Conductivity-temperature-depth (CTD)/dissolved O<sub>2</sub> casts were made at each station using either a Seabird SBE25 (R/V *Cape Ferguson*) or Seabird 911plus/SBE43 O<sub>2</sub> sensor (R/V *Melville*). Surface, middepth, and near-bottom water samples were obtained on the upcast using 10 L Niskin bottles, individually or in a rosette. In some cases, a Niskin was mounted at the base of a sediment multicorer to obtain bottom water within <30 cm of the seabed (R/V *Melville*). Winkler titrations on selected unfiltered samples were used to check the calibration of O<sub>2</sub> sensors. Water was filtered through 0.2 μm pore size Whatman Puradisc25 AS polyethersulfone inline filters for nutrient and δ<sup>13</sup>C-ΣCO<sub>2</sub> (dissolved inorganic carbon) analyses. Samples for Δ<sup>14</sup>C-ΣCO<sub>2</sub> analyses were unfiltered. Samples were transferred under a stream of N<sub>2</sub> into 2 mL or 10 mL glass ampoules (previously roasted 6 h at 450°C), flame sealed, and frozen (~20°C) for later isotopic analyses of ΣCO<sub>2</sub>.

#### 3.2. Seabed

[12] The seabed was sampled using a combination of gravity, kasten, multicorer, and piston corers. A wide-diameter gravity corer (15 cm ID, cellulose acetate butyrate (CAB) tubing) (R/V *Cape Ferguson*) or 8X multicorer (R/V *Melville*) were used to obtain the upper 0.5 m of the bottom for high-resolution sampling (1 to 5 cm depth intervals) and incubations of undisturbed material near the sediment-water interface. The gravity corer, configured with 2-m-long CAB barrels, or kasten corer (stainless steel barrels, 15 × 15 cm × 3 m and 12 × 12 × 3 m) were used to sample the upper 0–3 m at 10 cm intervals [Kuehl et al., 1985; Brunsell et al., 2002]. The piston corer (6.5 cm ID) sampled lengths up to

8 m, and cores were selectively subsectioned over 10 cm intervals.

### 3.2.1. Pore Water

[13] Sediment cores were subsampled without occluded air using 60 mL cutoff plastic syringes as minipiston corers. Detailed handling procedures for each core type followed *Aller et al.* [2004]. Subcores were extruded under N<sub>2</sub> into acid-washed (1N HCl) and distilled-water-rinsed 50, 125, or 250 mL centrifuge tubes or bottles, capped, and centrifuged at 5000 rpm (~4100 G) for 10–15 min using a gimbaled Sorval SS3 centrifuge and GSA rotor. Pore water was removed under N<sub>2</sub> into rubber-free plastic syringes through a short section of Tygon tubing and filtered through 0.2  $\mu\text{m}$  pore size Puradisc25 AS inline filters directly into a second rubber-free plastic syringe without exposure to air. The filtered pore water was divided and stored in plastic vials as acidified (to ~0.1 N HCl), unacidified (refrigerated), or frozen subsamples for a range of analyses, including  $\Sigma\text{CO}_2$  analyses onboard ship. Filtered pore water for  $\delta^{13}\text{C}$ - $\Sigma\text{CO}_2$  determination was transferred under N<sub>2</sub> into 2 mL glass ampoules, sealed, and stored frozen as described for overlying water. For selected depth intervals, a portion of centrifuged but unfiltered pore water was transferred into 10 mL glass ampoules, sealed and stored frozen for combined  $\delta^{13}\text{C}$ ,  $\Delta^{14}\text{C}$ - $\Sigma\text{CO}_2$  determinations. Great care was taken to avoid possible contamination with modern C sources at every handling step.

[14] When sediment gas was evident, piston core samples for CH<sub>4</sub> analysis were subsampled with 60 mL cutoff plastic syringes, and the wet sediment sections extruded under N<sub>2</sub> directly into 4 oz glass jars. Twenty milliliters of N<sub>2</sub> degassed distilled water was added under a flow of N<sub>2</sub>, the jars sealed with metal lids, and the samples frozen for later CH<sub>4</sub> concentration and  $\delta^{13}\text{C}$ -CH<sub>4</sub> analyses.

### 3.2.2. Sediment Incubations

[15] Net remineralization rates of  $\Sigma\text{CO}_2$  in surface sediment (0–20 cm) were determined at 28°C using time series incubations of both whole cores and individual sediment sections. Two to three glass tubes (4 cm ID, 25 cm length) were used to vertically subcore the upper 0–20 cm of sediment at each site for measurement of  $\Sigma\text{CO}_2$  production [*Aller et al.*, 1996]. The tubes were capped and placed in gas impermeable metallized plastic bags containing food-grade O<sub>2</sub> scrubbers, heat sealed, and stored at ambient air temperature (~28°C). These subcores were sectioned in 2 cm intervals and sampled for pore water and solids (as described subsequently) within 5–14 d, and then again after 20–50 d, depending on the build up rate of decomposition products. A diffusion-reaction model was utilized to calculate the optimal  $\Sigma\text{CO}_2$  production rate function versus depth from the time-dependent pore water profiles in the incubated cores, assuming a free solution diffusion coefficient for HCO<sub>3</sub><sup>−</sup> of 1.02 cm<sup>2</sup> d<sup>−1</sup> [*Aller et al.*, 1996; *Boudreau*, 1997]. In some cases, serial anoxic incubations of individual 10 cm intervals were sampled without additional depth resolution of pore water profiles, and the depth-integrated production rates of  $\Sigma\text{CO}_2$  within the 10 cm intervals determined from the slope of a  $\Sigma\text{CO}_2$  concentration versus time plot (2–16 weeks).

### 3.2.3. Sediment Solids

[16] Subsamples of sediment were stored in sealed 25 mL vials for water content and porosity determinations. Fol-

lowing the removal of pore water, residual sediment was retained in respective centrifuge bottles and frozen for later analyses.

[17] Cores for radiochemical analyses were sectioned at 2 cm intervals through the upper 20 cm and 4 cm intervals thereafter. Sediment samples were stored in double plastic bags in the dark before further processing for  $\gamma$  counting.

[18] Sedimentary structures at each site were documented using X radiography of core sections obtained by vertical insertion of acrylic tray subcorers (2.5 × 12 cm in cross section) into gravity and kasten cores.

## 4. Methods

### 4.1. Pore Water

[19] The initial  $\Sigma\text{CO}_2$  was measured on board ship and in all incubation samples using flow injection analysis/conductivity detection with a typical precision of ~2% (standard deviation relative precision) [*Hall and Aller*, 1992]. Cl<sup>−</sup> was determined with 1% precision on unacidified samples using a Radiometer CMT 10 titrator. Total dissolved S (SO<sub>4</sub><sup>2−</sup>) was analyzed in acidified pore water using Inductively Coupled Plasma Atomic Emission Spectroscopy (ICP-AES) (Varion Liberty 200), precision 3%, and a subset checked for equivalence to SO<sub>4</sub><sup>2−</sup> using ion chromatography (HCO<sub>3</sub><sup>−</sup>/CO<sub>3</sub><sup>2−</sup> eluent, Dionex AS4A column). Dissolved Fe and Mn were determined colorimetrically using ferrozine and formaldoxime, with precisions of ~2–3% [*Stookey*, 1970; *Goto et al.*, 1962] and using ICP-AES.

[20] Water samples for  $\Sigma\text{CO}_2$  isotopic analyses were treated as described by *Aller and Blair* [2006]. For some samples, 0.1–0.4 mL of pore water were injected into preflushed, sealed 3 mL Wheaton vials containing the H<sub>3</sub>PO<sub>4</sub>/CuSO<sub>4</sub> mixture. The CO<sub>2</sub> was stripped with helium, dried via passage through MgClO<sub>4</sub> and Nafion™ tubing (Perma-Pure), and delivered to a Conflo III open split interface connected to a Thermo Delta V IRMS for  $\delta^{13}\text{C}$  measurements. Samples for  $\Delta^{14}\text{C}$ - $\Sigma\text{CO}_2$  measurements (10 mL ampoules) were treated as described by *Aller and Blair* [2004]. Splits of these samples were also used for  $\delta^{13}\text{C}$  measurements. Graphite conversions and  $^{14}\text{C}$  analyses were made by the National Ocean Sciences Accelerator Mass Spectrometry (AMS) Facility at the Woods Hole Oceanographic Institution. The  $^{14}\text{C}$  contents are reported as the fraction modern relative to the National Bureau of Standards (NBS) Oxalic Acid I standard or as  $\Delta^{14}\text{C}$  [*Olsson*, 1970; *Stuiver and Polach*, 1977]. Modern is defined as 95% of the radiocarbon concentration (in A.D. 1950) of the NBS standard normalized to a  $\delta^{13}\text{C}$  of −19‰ [*Olsson*, 1970]. Corrections for natural fractionations were made by normalizing the  $\delta^{13}\text{C}$  values of the samples to −25 ‰. The relative precisions for the NBS-22 hydrocarbon standard were 12% for fraction modern and 2% for  $^{14}\text{C}$  age.

[21] Methane samples were homogenized and headspace samples removed using a can-piercing sampler. Methane was determined using a Shimadzu Mini2 GC equipped with a Valco 6-port loop injector, a 1/8" o.d. × 3' long molecular sieve 5A column (100–120 mesh) maintained at room temperature and a flame ionization detector operated at 250°C. Gas samples were also processed through a combustion line (CuO at 780–790°C) [*Chanton and Martens*,

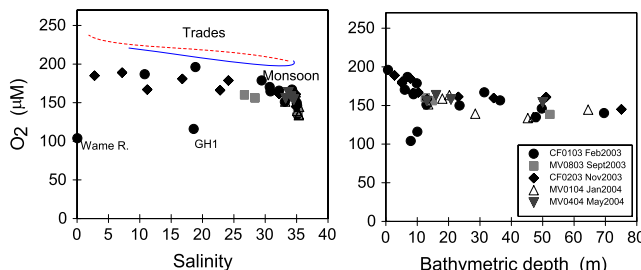


**Figure 2.** Overlying water column was generally well oxygenated at all times of year throughout the clinoform system (>75% saturation), as illustrated by bottom water  $\text{O}_2$  concentrations as a function of (left) salinity or (right) bathymetric depth. The dashed (monsoon) and dotted (trades) lines connect the range of  $\text{O}_2$  saturation concentrations at the temperatures and salinities of the sampling sites (generally lower temperatures during trades). Bottom water in the Wame River mangrove-lined, distributary channels (Aird-Purari delta region) showed the greatest depletion (<50% saturation).

1988], and the resulting  $\text{CO}_2$  purified for isotopic measurements as described previously.

#### 4.2. Sediment

[22] Weighed sediment samples for  $\text{C}_{\text{org}}$  isotopic analyses (particulate organic carbon) were treated with 4N HCl for 4 d at room temperature to remove carbonates, dried under vacuum, and reweighed. Subsamples were placed in tin boats and analyzed for  $\text{C}_{\text{org}}$  and N concentrations ( $\text{mg g}^{-1}$  dry wt sample) with a Carlo Erba 1108 CHNS analyzer. Precision was 2%. The  $\text{CO}_2$  produced via the oxidation of the  $\text{C}_{\text{org}}$  was trapped cryogenically for both  $^{13}\text{C}/^{12}\text{C}$  and  $^{14}\text{C}/^{12}\text{C}$  analyses as described previously for water samples. The most recent POC  $\delta^{13}\text{C}$  analyses were made using a CE 1112 EA interfaced to a Thermo Delta V IRMS.  $\text{C}_{\text{org}}$ , total C, and total N were measured on additional samples using a Perkin Elmer 2400 CHNS/O Series II Analyzer and a Shimadzu TOC-5000, the latter after sample acidification, precision typically 3–5%. Carbonate carbon was determined by difference between the total carbon before and after acidification.

[23] In some cases, organic carbon concentrations were normalized to the specific surface area of the sample to minimize variations due strictly to grain size and differential transport rather than net reaction [Mayer, 1994a, 1994b; Hedges and Keil, 1995]. Subsamples of the sediment were rinsed with deionized water to remove salts, dried and then roasted in air for 12–14 h at 350°C. After degassing at 150°C for 30 min., the surface area was determined by the multipoint method on a Beckman Coulter SA 3600 analyzer. Precision of the measurements was 2%.

[24] Highly reactive Fe minerals and Fe oxidation states were estimated by leaching freshly thawed, wet sediment for 15 min in 6N HCl at 22°C. Total highly reactive Fe and Fe(II) were measured immediately after leaching using ferrozine with and without hydroxylamine reductant [Aller and Blair, 1996; Viollier et al., 2000]. A separate sample was used to determine dry/wet ratios for conversion of concentrations to dry weight basis. Al was determined using

sediment or suspended matter digestion with concentrated  $\text{HNO}_3$  and  $\text{HClO}_4$  for 3 h at 120°C and then refluxed 3 h at 180°C to eliminate  $\text{HNO}_3$ . Standards were prepared in a comparable solution matrix.

[25] Measurements of  $^{210}\text{Pb}$ ,  $^{226}\text{Ra}$ , and  $^{137}\text{Cs}$  were made at AIMS on 50–150 g of dried and ground sediment packed into gas-tight Perspex containers. Gamma counting was done using one well and four planar germanium detectors in lead-shielded castles. Estimation of  $^{210}\text{Pb}$  used the 46.5-keV gamma emission. After radon daughter ingrowth (3–4 weeks),  $^{226}\text{Ra}$  was determined from the gamma emission of  $^{214}\text{Pb}$  at 295 and 351 keV, and  $^{214}\text{Bi}$  at 609 keV. The  $^{137}\text{Cs}$  was estimated from the 661.6-keV gamma emission of  $^{137m}\text{Ba}$ . Energy spectra were calibrated with Amersham and CANMET low-activity standards in cleaned silica sand of geometry and mass comparable to the sediment samples. International Atomic Energy Agency (IAEA) marine sediment reference material IAEA-315 was used to check calibrations. Total propagated counting errors were ~5–10%, except for very low activity  $^{137}\text{Cs}$  samples where errors were ~30%. Only  $^{137}\text{Cs}$  activities >1.5 times the total propagated error were considered detectable (>0).

[26] Sediment sections were X-radiographed in acrylic trays using a Kramex portable X-ray unit (20 mA 60 kV<sup>-1</sup>) and Fujifilm IX industrial X-ray film.

## 5. Results

### 5.1. Water Column

[27] CTD casts showed minor seasonal ranges of bottom water temperatures and salinities from 26.2 to 27.7°C and 35 to 35.2, respectively, at GH75, the most seaward bottomset site. Topset bottom temperatures varied more substantially from 26.8 to 29.5°C, with salinities ranging from 16 over the inner (5 m) to 35 on the outer topset (25 m). As exemplified by GH14, topset bottom waters tended to be warmer during the NW monsoon (29.5°C) relative to trades (27.2°C), and, at some sites, more saline [Aller et al., 2008]. Bottom waters were well oxygenated throughout the gulf during all seasons, with topset and foreset concentrations 160–180  $\mu\text{M}$  (~75 to >80% saturation), in general agreement with previous observations (Figure 2) [Mitchell, 1982; Aller et al., 2004]. Oxygen in surface waters ranged from 180 to 200  $\mu\text{M}$ . The lowest  $\text{O}_2$  concentrations and coldest temperatures were found in the bottom water in channels of the Wame River in the Aird (Purari) delta (100–120  $\mu\text{M}$ ; T = 23°C). The lowest  $\text{O}_2$  layers within the water column on the foreset (40–50 m) correlated with decreased light transmission (suspended matter). Detailed examples of water column property profiles at or near the coring sites are given by McKinnon et al. [2007], Ogston et al. [2008], and Aller et al. [2008].

### 5.2. Sediment Properties and Diagenetic Environment

#### 5.2.1. Sedimentary Structures

[28] Previous studies demonstrated a general dominance of physically formed sedimentary structures and lack of well-developed macrobenthic communities within tidal channels and across much of the topset region in the central gulf between depths of ~5 and 20 m [Alongi et al., 1992; Alongi and Robertson, 1995; Walsh et al., 2004; Aller and Aller, 2004; Dalrymple et al., 2003; Goñi et al., 2008].

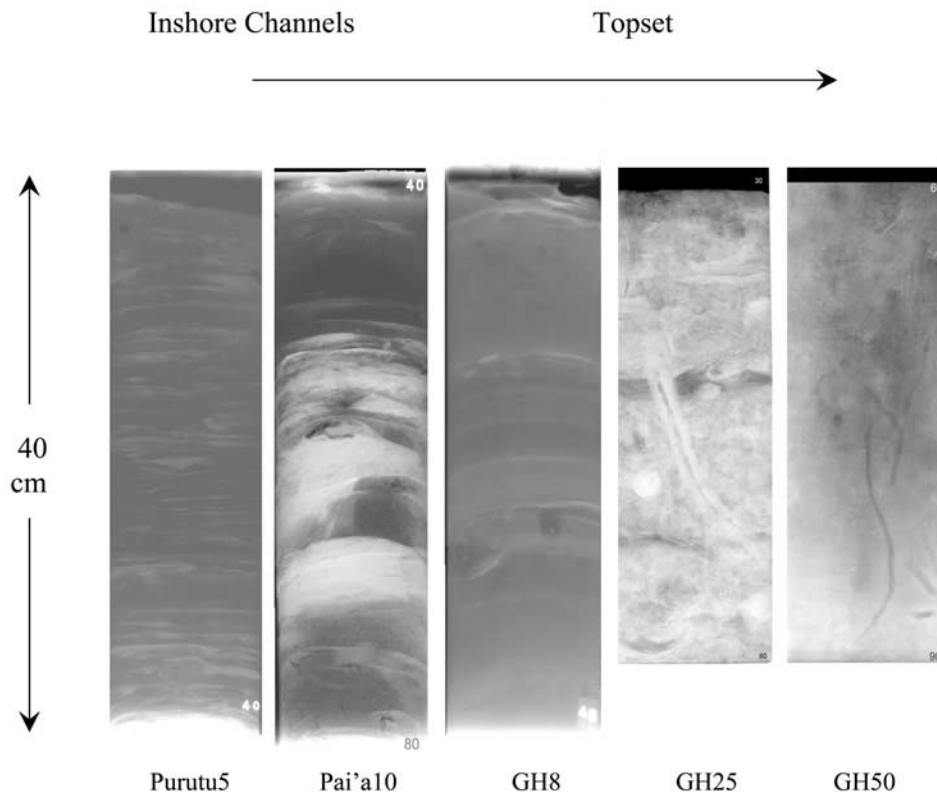


**Figure 3.** Representative X-radiographs of sedimentary structures at inshore distributary channels (Purutu5, Fly River delta plain, 0–40 cm; Pai'a10, Pai'a inlet, Purari delta plain, 40–80 cm), inner topset (GH8, central gulf, 0–40 cm), outer topset (GH25, central gulf, 30–60 cm) and foreset (GH50, central gulf, 60–90 cm) sites illustrate the typical regular pattern of domination by physically formed structures in channel and topset deposits inshore (interbedded muds, sands), and the increasing dominance of macrobenthic biogenic structures offshore. (X-ray negative images, lightly colored regions contain sediment with relatively high bulk densities [see also *Alongi et al.*, 1992; *Walsh et al.*, 2004; *Dalrymple et al.*, 2003; *Aller and Aller*, 2004].) The dark flecks visible below ~50 cm in the Pai'a10 X-radiograph are formed by methane bubbles and are commonly observed below the physically reworked layer in the channel bed and topset deposits.

Interbedded sands and muds characterize the inshore (<10 m), with sand deposits and shoals common off the river mouths and within tidal channels. Sandy layers become progressively subordinate to silt and clay offshore (5–20 m), but increase again within the outer topset (25–35 m) [Walsh *et al.*, 2004]. Watery, tidally mobile muds often overlie the sandy channel bottoms, or are present as a transient drape over sandy intertidal flats. The available coring gear did not permit sampling of relatively sandy bottoms, and thus seabed sampling is biased to muddy deposits. Truncated biogenic structures and tubicolous benthic species are occasionally present in the mud deposits of the topset; evidence of episodic but temporary colonization of an otherwise physically reworked seabed by macrobenthos [*Alongi et al.*, 1992; *Aller and Aller*, 2004]. Biogenic structures, and the macrobenthos that form them, become progressively more common at depths >20 m on the outer topset, and dominate sedimentary fabric in the foreset and bottomset [Walsh *et al.*, 2004; *Aller et al.*, 2008]. These overall patterns were evident at the range of inshore–offshore sites sampled in the present study. Representative

examples from areas or sampling times that were not included in earlier reports are shown in Figure 3. One feature not emphasized in previous reports is the common occurrence of methane gas-bubble structures below ~40–100 cm depth in the tidal channels and topset deposits (Figure 3). These gas-rich zones were usually found in relatively consolidated, firm muds unconformably underlying a more watery and visually oxidized surface layer (Fe oxide rich) between 10 and 40 cm thick.

### 5.2.2. Radiochemical Distributions

[29] The distributions of  $^{210}\text{Pb}$  and  $^{137}\text{Cs}$  distributions varied substantially between the sampling regions, indicative of the variety of sedimentation regimes within the subaqueous area. As illustrated by station GH50, the foreset and bottomset facies were characterized by exponentially decreasing excess  $^{120}\text{Pb}$  ( $^{210}\text{Pb}_{\text{xs}}$ ) and smoothly varying  $^{137}\text{Cs}$  activities (Figure 4), implying a relatively steady supply and accumulation of debris. Sedimentary structures and detailed examination of the activity distributions indicate that on the central gulf foreset, deposition likely takes place episodically in layers 5–10 cm thick, but sufficiently

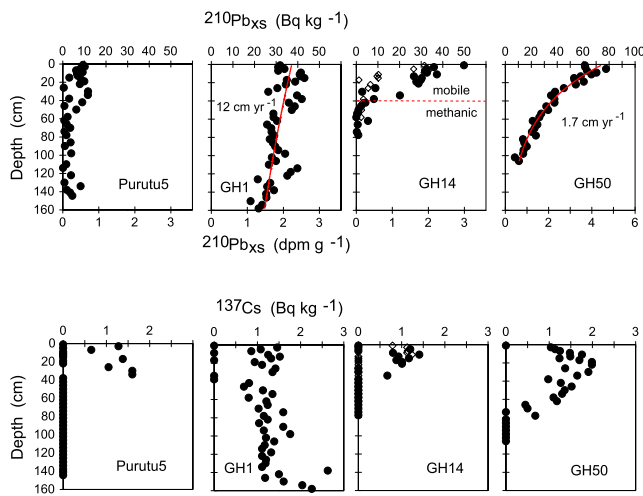


**Figure 4.** Example vertical profiles of excess  $^{210}\text{Pb}$  ( $^{210}\text{Pb}_{\text{xs}}$ ) and  $^{137}\text{Cs}$  activities illustrate the widely ranging, but regularly varying, depositional conditions found across the delta facies inshore approaching offshore. Purutu5 (mangrove distributary channel, Purutu Island, Fly delta) has low activities of  $^{210}\text{Pb}_{\text{xs}}$  characteristic of river suspended matter and shows evidence of episodic deposition. GH1 (Wame River channel, Aird-Purari delta) has high activities of  $^{210}\text{Pb}_{\text{xs}}$  characteristic of open shelf deposits and shows extremely rapid accretion of a channel bar (advection model fit  $\sim 12 \text{ cm a}^{-1}$ ). GH14 (midtopset, central gulf) has a physically reworked, seasonally variable surface layer,  $\sim 35 \text{ cm}$  thick at the time of 2003 trades sampling (solid symbols) and  $\sim 10 \text{ cm}$  thick during the 2003 monsoon (solid symbols). The mobile layer unconformably overlies firmer, methanic deposits that lack  $^{210}\text{Pb}_{\text{xs}}$  and detectable  $^{137}\text{Cs}$  (indicated by horizontal line). GH50 (foreset, central gulf) shows approximately exponential decrease of  $^{210}\text{Pb}_{\text{xs}}$  with depth, implying steady accumulation at an average rate of  $\sim 1.7 \text{ cm a}^{-1}$ , although as suggested by adjacent sampling intervals of near constant activity and X-radiographs, sediment appears to accumulate in episodic pulses of 5–10 cm [see also Walsh et al., 2004; Aller and Aller, 2004].

regularly so as to produce an overall time-averaged steady accumulation (GH50,  $1.7 \text{ cm a}^{-1}$ ; Figure 4), in the range expected based on general spatial patterns [Brunskill et al., 2003, 2007b; Walsh et al., 2004]. Net accumulation decreases substantially on the bottomset (GH75,  $\leq 0.56 \text{ cm a}^{-1}$ ; data not shown), and activity distributions are strongly influenced by bioturbation, making estimates of accumulation maxima if only steady advective transport is assumed to affect the  $^{210}\text{Pb}_{\text{xs}}$  distribution. In contrast to the foreset and bottomset, sites on the inner topset region ( $< 20 \text{ m}$ ) typically have a seasonally variable surficial layer of sediment  $\sim 10$ – $40 \text{ cm}$  in thickness with relatively uniform or sometimes irregular  $^{210}\text{Pb}_{\text{xs}}$  and  $^{137}\text{Cs}$ . The layer unconformably overlies firm sediment lacking analytically significant activities (e.g., GH14, Figure 4); GH8, H5, HI5 (data not shown) (see also examples from Brunskill et al. [2003] and Walsh et al. [2004]). This surficial layer is physically reworked sufficiently often that no steady  $^{210}\text{Pb}_{\text{xs}}$  or  $^{137}\text{Cs}$  activity gradients are formed relative to analytical error, compromising estimates of net accumulation, if it occurs.

[30] The inshore tidal channels and channel bars within the Fly and Aird-Purari delta plains show evidence of episodic, sometimes extremely rapid, deposition (Purutu5, GH1, Figure 4) [see also Walsh and Nittrouer, 2004]. Interpreted as steady accumulation, the  $^{210}\text{Pb}_{\text{xs}}$  distribution at GH1 indicates accretion rates of  $\sim 12 \text{ cm a}^{-1}$ ; however, this migrating channel bar deposit is clearly transitory. Of significant importance is the fact that  $^{210}\text{Pb}_{\text{xs}}$  activities at GH1 (Aird-Purari delta) are high and comparable to the offshore marine topset and foreset regions ( $30$ – $40 \text{ Bq kg}^{-1}$ ); whereas at Purutu5 (Fly delta plain),  $^{210}\text{Pb}_{\text{xs}}$  activities are 4–5 times lower ( $\leq 10 \text{ Bq kg}^{-1}$ ) and equivalent to activities in riverine suspended sediment [Brunskill et al., 2007a; Aalto et al., 2008].

### 5.2.3. Sediment C, C/N, and Al

[31] Average sediment  $\text{C}_{\text{org}}$  and C/N over the upper 1–2.5 m at the sampling sites varied between  $0.6$ – $2 \text{ mmol C}_{\text{org}} \text{ g}^{-1}$  and  $9.3$ – $16.2 \text{ mol mol}^{-1}$ , respectively, with most seabed sites  $0.8$ – $1.4 \text{ mmol g}^{-1}$  and  $9$ – $13 \text{ mol mol}^{-1}$  (Table 2). Carbonate C ( $\text{C}_{\text{inorg}}$ ) ranged between  $0.07$  and  $0.47 \text{ mmol g}^{-1}$  ( $0.7$ – $4.7\%$   $\text{CaCO}_3$  dry weight) with lowest values at the inner topset sites GH8 and H5, and the highest at the bottomset site GH75 (Table 2). Suspended matter collected at zero salinity in the Fly River and Wame River (Aird-Purari delta) ranged from  $0.87$  to  $0.94 \text{ mmol C}_{\text{org}} \text{ g}^{-1}$  and  $12.3$  to  $13.8 \text{ C/N}$ ; and suspended matter at the mouth of the Turama was  $1.19 \text{ mmol g}^{-1}$  with  $\text{C/N} = 13.2$ . These ranges agree well with other studies [Bird et al., 1995; Brunskill et al., 1995; Aller and Blair, 2004; Goñi et al., 2006, 2008]. The highest  $\text{C}_{\text{org}}$  ( $2 \text{ mmol g}^{-1}$ ) and C/N ( $16.2$ ) values were found at the tidal channel bar site GH1 in the Aird-Purari delta plain. Vertical profiles of sediment  $\text{C}_{\text{org}}$  and C/N demonstrated that, except at the inner topset and channel sites where the presence of distinct sand layers locally lower  $\text{C}_{\text{org}}$ , these values showed very little variation with depth at most stations (Figure 5) [see also Alongi et al., 1992; Aller and Blair, 2004; Goñi et al., 2008]. A regular decrease, however, of  $\text{C}_{\text{org}}$  from  $0.9$  to  $0.7 \text{ mmol g}^{-1}$  was observed with depth at foreset site GH50, suggestive of progressive diagenetic loss (Figure 5; implies remineralization  $\sim 55 \mu\text{mol C m}^{-2} \text{ d}^{-1}$ ). The lowest  $\text{C}_{\text{org}}$  was found at GH25, where relatively sand-rich deposits characteristic of the scoured outer topset occur [Walsh et al., 2004], and where Al content, which largely reflects fine-grained clay mineral content, was lowest ( $2 \text{ mmol g}^{-1}$ ). Although  $\text{C}_{\text{org}}$  content is poorly correlated with Al within the relatively restricted station set examined here (Table 2), a general relationship obtained from 69 surface sediment samples taken throughout the gulf during February and November 2003 is  $\text{C}_{\text{org}} = 0.171 * [\text{Al}]^{1.89}$  ( $\text{mmol g}^{-1}$ ) (data not shown,  $r^2 = 0.81$ ;  $P < 0.001$ ) includes all stations in Table 2).

[32] Bulk sediment surface areas (SA) varied between  $10.4 \text{ m}^2 \text{ g}^{-1}$  (GH8,  $90$ – $100 \text{ cm}$ ) and  $33.4 \text{ m}^2 \text{ g}^{-1}$  (GH8,  $30$ – $40 \text{ cm}$ , surface mobile layer), the extremes occurring within different depth intervals of interbedded muds and sands at the same inner topset site GH8. The highest SAs were otherwise found inshore at GH1 (mangrove channel bar) and on the foreset-bottomset (GS48; GH75). Much of the inner and midtopset is characterized by bulk sediment SAs between  $20$  and  $25 \text{ m}^2 \text{ g}^{-1}$  [Goñi et al., 2008; Aller and Blair, 2004] (Table 2). SA ( $\text{m}^2 \text{ g}^{-1}$ ) correlates directly with Al content ( $\text{mmol g}^{-1}$ ), giving a geometric mean

**Table 2.** Seabed and Suspended Matter Properties<sup>a</sup>

Station	Interval, cm	C <sub>org</sub> , mmol g <sup>-1</sup>	C/N, mol mol <sup>-1</sup>	C <sub>inorg</sub> , mmol g <sup>-1</sup>	Al, mmol g <sup>-1</sup>	C <sub>org</sub> δ <sup>13</sup> C ‰ (PDB)	Cl <sup>-</sup> , mM	SA, m <sup>2</sup> g <sup>-1</sup>	C <sub>org</sub> /m <sup>2</sup> mg m <sup>-2</sup>	
Fly River	surface	0.77	12.2	0.21	2.30	-26.87	0	salinity	16.48	0.56
Wame River	surface	0.88	10.7	0.08	2.84	-25.37	0	salinity	22.37	0.47
Turama River (mouth)	bottom	1.19	13.6	0.05	2.41	-27.00	<2	salinity	28.08	0.51
GH1	0–160	2.01 ± 0.22	16.2 ± 1.7	0.294 ± 0.108	2.84 ± 0.15	-27.58	159 ± 19	30.11	0.80	
Purutu5	0–147	0.813 ± 0.12	12.7 ± 1.7	0.136 ± 0.028	2.45 ± 0.22	-26.77	290 ± 34	19.79	0.49	
Pai'a10	0–166	1.45 ± 0.44	13.69 ± 1.78	0.241 ± 0.117	2.72 ± 0.52	-27.68	184 ± 24	36.36	0.48	
H5	0–140	1.122 ± 0.129	11.5 ± 2.27	0.069 ± 0.035	2.90 ± 0.40	-24.6 <sup>b</sup>	289 ± 13	22.5 <sup>b</sup>	0.60	
HI-5	0–111	0.819 ± 0.278	12.3 ± 2.5	0.121 ± 0.054	2.59 ± 0.37	-26.5 <sup>b</sup>	351 ± 21			
GH8	0–168	1.02 ± 0.28	13.23 ± 2.1	0.079 ± 0.059	2.85 ± 0.32	-26.78 ± 0.15 <sup>c</sup>	360 ± 22	24.3 ± 9.1 <sup>c</sup>	0.49 ± 0.05	
GH14 (monsoon)	0–111	1.11 ± 0.35	13.6 ± 2.3	0.111 ± 0.061	2.80 ± 0.36	-27.04	487 ± 11	29.73	0.45	
GH14 (trades)	0–110	1.23 ± 0.28	14.1 ± 2.6	0.078 ± 0.041	3.06 ± 0.33	-26.79	467 ± 12	30.39	0.49	
GH25	0–132	0.602 ± 0.123	12.1 ± 2.02	0.429 ± 0.050	2.06 ± 0.15	-26.37	542 ± 15	24.99	0.29	
GH35 (M)	0–168	0.883 ± 0.049	11.44 ± 1.1	0.127 ± 0.031	2.83 ± 0.12	-25.94	548 ± 6	32.09	0.33	
GH50	0–172	0.820 ± 0.039	9.27 ± 0.60	0.150 ± 0.026	3.16 ± 0.22	-25.60 ± 0.13 <sup>c</sup>	555 ± 4	23.1 ± 1.3 <sup>c</sup>	0.42 ± 0.05	
GS48 (HM50)	0–250	1.387 ± 0.312	12.8 ± 1.70	0.189 ± 0.034	2.93 ± 0.15	-27.08 <sup>c</sup>	547.5 ± 5	31.5 <sup>c</sup>	0.53	
GH75	0–136	0.868 ± 0.099	9.44 ± 0.53	0.469 ± 0.12	3.13 ± 0.12	-23.70	556 ± 4	31.6	0.33	

<sup>a</sup>The δ<sup>13</sup>C and SA from 0 to 10 cm, all other properties, including pore water Cl<sup>-</sup>, averaged over entire core depth interval unless indicated.

<sup>b</sup>From same or nearby station of Goñi et al. [2008].

<sup>c</sup>Mean of the five intervals listed in Table 3.

regression over the restricted ranges 10–34 m<sup>2</sup> g<sup>-1</sup> and Al = 2–3 mmol g<sup>-1</sup>, SA = 26.7[Al] – 50.9; ( $r^2 = 0.44$ ; P = 0.014) or, assuming a nonlinear fit passing through the origin SA = 1.8[Al]<sup>2.47</sup>. The correlations between C<sub>org</sub>, SA, and Al demonstrate the importance of the fine-grained fraction dominated by clay minerals in determining the distribution of C<sub>org</sub>. The average C<sub>org</sub>/SA ratio expected in surface sediments based on the C<sub>org</sub> and SA correlations with mineral Al over the Al range 2–3.25 mmol g<sup>-1</sup> is 0.64 mg C<sub>org</sub> m<sup>-2</sup> (i.e., ratio of C<sub>org</sub>(Al) and SA(Al) averaged over Al concentration). Significant deviations from this predicted mean loading ratio occur, with elevated measured ratios at the mangrove channel site GH1 (0.8 mg C<sub>org</sub> m<sup>-2</sup>) and lower measured ratios at the foreset and bottomset sites GH50 and GH75 (0.4 to 0.3 mg C<sub>org</sub> m<sup>-2</sup>).

#### 5.2.4. C<sub>org</sub> Isotopic Distributions

[33] River surface suspended matter samples from zero-salinity end-members in the Fly River and Wame River (Aird-Purari delta) gave C<sub>org</sub> δ<sup>13</sup>C values of -26.87 and -25.37 ‰, respectively (Table 2). The Fly River value, which was derived from a ~1000 L sample, agrees well with those reported by Keil et al. [1997] for suspended matter (-26.77 ± 0.25 ‰) and for the river bed (-26.85 ± 0.1‰) by Bird et al. [1994, 1995]. Goñi et al. [2006] measured lighter values at two sites in the Fly apex region -29.8 and -29.3‰, possibly reflecting local input of mangrove detritus. The value measured here for the Wame River is comparable to those found in surface soil humic layers in the regional upland drainage basin (Purari), however, reported soil values were from samples that purposely discriminated against mineral material common (as indicated by Al) in river suspended samples [Bird et al., 1994]. The Turama River mouth sample, -27.00‰, was obtained at a salinity greater than zero.

[34] Seabed bulk C<sub>org</sub> δ<sup>13</sup>C samples were analyzed from the 0–10 cm depth interval at a subset of the stations. Values varied from a low of -27.55‰ at GH1 (mangrove/Nypa palm fringed tidal channel), to a high of -23.70‰ at GH75 (bottomset) (Table 2). Inner and midtopset sites (5–20 m) range between -27.2‰ (GH14) and -26.8‰ (GH8),

consistent with typical values of -26.5 ± 0.1‰ measured over much of the topset in the more extensive spatial studies of Bird et al. [1995] and Goñi et al. [2008] and the topset sites of Aller and Blair [2004]. The progressive increase in bulk C<sub>org</sub> δ<sup>13</sup>C across the foreset (-25.6‰; GH50) and bottomset (-23.5‰; GH75), either without significant change or with a decrease in total C<sub>org</sub> also agrees with the general depth-dependent patterns resolved previously [Bird et al., 1995; Brunskill et al., 1996].

[35] Down-core variation in C<sub>org</sub> δ<sup>13</sup>C over depths of 2–6 m is minimal at representative inner topset site GH8 and foreset site GH50, in agreement with measurements at most, but not all, inner topset and foreset locations reported to date [Aller and Blair, 2004; Goñi et al., 2008]. In contrast, C<sub>org</sub> Δ<sup>14</sup>C decreases substantially at both GH50, where there is an initial progressive change with depth and then an apparent stabilization of Δ<sup>14</sup>C around ~-500‰ (5500–6350 years) between 4 and 6 m. At inner topset site GH8, C<sub>org</sub> Δ<sup>14</sup>C has a stepwise distribution consistent with a two-layer diagenetic regime: a reworked surface layer 0–40 cm thick having mean C<sub>org</sub> age ~2500 years within which

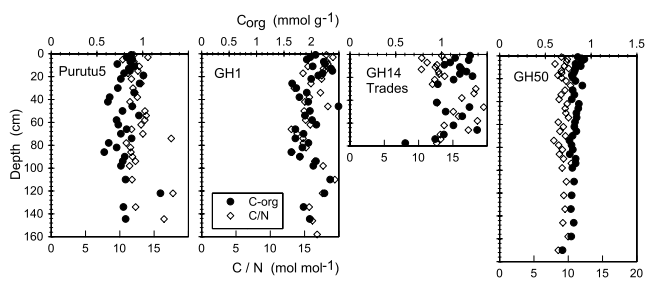


**Figure 5.** Vertical changes in C<sub>org</sub> concentration and C/N ratios are minimal in the upper ~2 m of sites examined in distributary channels and on the topset, with variations largely related to grain size differences between interbedded mud and sand layers [see also Goñi et al., 2008]. Small but regular decreases in C<sub>org</sub> with depth on the foreset imply slow, progressive diagenetic loss (e.g., GH50 ↔ 55 μmol m<sup>-2</sup> d<sup>-1</sup> over upper 2 m, k = 0.019 a<sup>-1</sup>).

**Table 3.** Inner Topset and Foreset  $^{14,13}\text{C}$  Vertical Profiles

Interval, cm	$\text{C}_{\text{org}}$ , mmol g $^{-1}$	$\text{C}_{\text{org}} \delta^{13}\text{C}$ (PDB), ‰	$\text{C}_{\text{org}} \Delta^{14}\text{C}$ , ‰	Fraction Modern	SA, m $^2$ g $^{-1}$	$\text{C}_{\text{org}}/\text{m}^2$ , mg m $^{-2}$
<i>GH8</i>						
0–10	1.47	−26.79	−371.3	$0.6287 \pm 0.0049$	31.15	0.57
30–40	1.28	−26.90	−476.6	$0.5234 \pm 0.0038$	33.51	0.46
70–80	0.95	−26.95	−503.6	$0.4964 \pm 0.0039$	24.03	0.47
90–100	0.38	−26.61	−546.3	$0.4537 \pm 0.0032$	10.35	0.44
150–160	0.93	−26.64	−498.6	$0.5014 \pm 0.0029$	22.60	0.49
<i>GH50</i>						
50–60	0.99	−25.69	−269.7	$0.7303 \pm 0.005$	24.97	0.48
140–150	0.85	−25.51	−273.7	$0.7263 \pm 0.0037$	22.55	0.45
275–285	0.70	−25.55	−399.2	$0.6008 \pm 0.0037$	21.67	0.39
365–375	0.67	−25.63	−557.2	$0.4428 \pm 0.0031$	22.46	0.36
592–602	0.84	−26.26	−436.4	$0.5636 \pm 0.0048$	24.06	0.42

$^{210}\text{Pb}_{\text{xs}}$  is homogeneous (data not shown), discontinuously overlying an older, methanic zone characterized by  $\text{C}_{\text{org}} > 4000$  years old (Table 3).

### 5.2.5. Pore Water $\text{SO}_4^{2-}$

[36] Dissolved  $\text{SO}_4^{2-}$  is initially available (see pore water  $\text{Cl}^-$  concentrations, Table 2) and depleted with depth at all sites, consistent with net diagenetic reduction (Figure 6). The depths of zero  $\text{SO}_4^{2-}$  at topset sites usually occur within  $\sim 0.5$ –1 m of the surface and are clearly associated with depositional and diagenetic discontinuities. These discontinuities are indicated by a sharp color change from light to dark, a jump in sediment firmness, visually evident erosional contacts, and obvious methanic compositions (gas bubbles) juxtaposed with the suboxic layer. The lack of substantial curvature in the  $\text{SO}_4^{2-}$  profiles (i.e., linearity) within the nonbioturbated, upper few decimeters of sediment on the topset implies that much of the reduction takes place near the lower boundary of the  $\text{SO}_4^{2-}$  gradient in

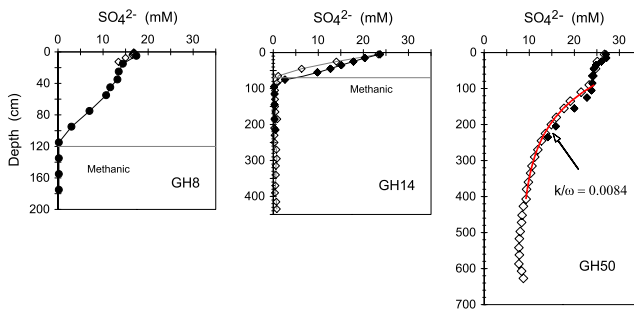


**Figure 6.** Pore water  $\text{SO}_4^{2-}$  profiles at topset sites, e.g., (left) GH8 and (middle) GH14, show approximately constant concentrations or linear decreases with depth, implying that net reduction of  $\text{SO}_4^{2-}$  is focused toward the base of the physically reworked surface layer, and that anaerobic oxidation of  $\text{CH}_4$  occurs near the basal depositional unconformity. (right) As illustrated by GH50, net reduction of  $\text{SO}_4^{2-}$  that takes place below the bioturbated zone in foreset deposits and  $\text{SO}_4^{2-}$  decreases exponentially to a constant, nonzero value over the sampled interval (the fitted curve represents the one-dimensional diagenetic model fit discussed in text with  $k/\omega = 0.0084 \text{ cm}^{-1}$ ,  $k = 0.014 \text{ a}^{-1}$ ). The two sets of symbols (open, solid) represent samples from different cores at the same sites (e.g., kasten and piston cores at GH14 and GH50; high-resolution and long gravity cores at GH8).

association with anaerobic  $\text{CH}_4$  oxidation. In contrast to topset sites, the foreset is characterized by extended zones of  $\text{SO}_4^{2-}$  reduction with nonzero terminal concentrations of  $\text{SO}_4^{2-}$  over the depth scales sampled by piston cores (6–8 m) (Figure 6).

### 5.2.6. Sediment Fe Distributions and Seasonal Dynamics

[37] Pore water Fe and solid phase reactive Fe oxidation states reflect suboxic diagenetic redox conditions and sedimentary dynamics in the study area, selected examples of which are given here for the topset site GH14 and foreset site GH50 (Figure 7). The topset site GH14 shows evidence of substantial seasonal variation in diagenetic conditions in the upper 15–30 cm, with relatively high subsurface dissolved Fe (100–250  $\mu\text{M}$ ) maxima and a high proportion of

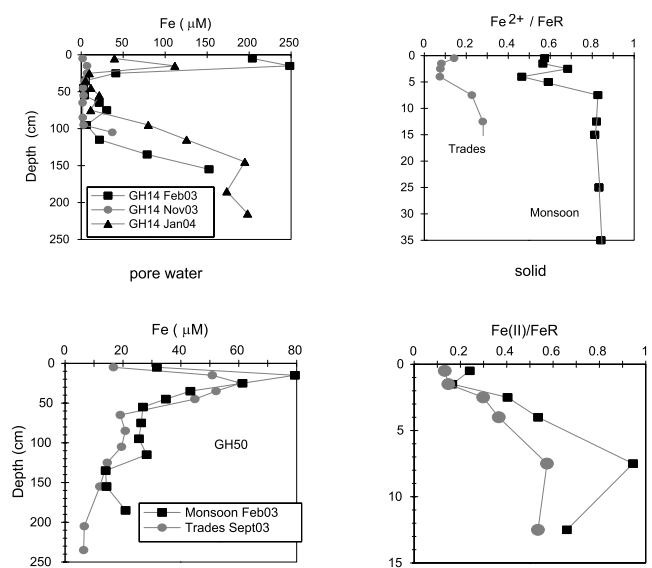


**Figure 7.** Pore water Fe and solid phase reactive Fe oxidation states at middle topset site GH14 vary seasonally, consistent with suboxic diagenetic conditions in the physically reworked surface zone, seasonal oxidation of reworked sediment during the trades period, and the ingrowth of reduced  $\text{Fe}^{2+}$  during the more quiescent monsoon period. Suboxic, nonsulfidic redox conditions also characterize the bioturbated zone at foreset site GH50, and any seasonal changes, if they occur, are relatively subdued compared to the topset.

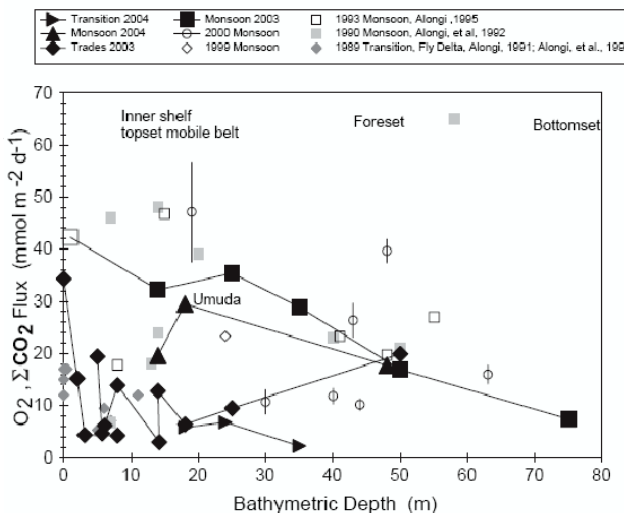


**Figure 8.** Benthic  $\Sigma\text{CO}_2$  production rates in the upper 0–20 cm ranged between  $\sim 3$  and  $43 \text{ mmol m}^{-2} \text{ d}^{-1}$  and varied substantially seasonally, particularly on the topset and in the Umuda Valley (solid symbols). The highest remineralization rates were measured during the monsoon periods, as were the highest concentrations of sedimentary Chl *a* [Aller et al., 2008]. Benthic  $\text{O}_2$  fluxes estimated in previous studies (before 2003; open or gray symbols) in the Fly delta and central gulf clinofor are also plotted and used in averages for  $\text{C}_{\text{org}}$  budgets [Alongi, 1995; Alongi et al., 1992, 1993; Aller et al., 2004].

reduced solid phase Fe ( $\text{Fe(II)}/\text{FeR} \sim 0.6$ – $0.8$ ) at all depths during the monsoon periods, and relatively oxidized solid phase Fe ( $\text{Fe(II)}/\text{FeR} \sim 0.2$ ) and low dissolved Fe ( $<20 \mu\text{M}$ ) in surface sediment during the late trades. The upper  $\sim 30$  cm of sediment was also visually oxidized and very watery in the trades cores, consistent with recent physical reworking, exposure to oxygenated overlying water, and reoxidation. In contrast, although the foreset site GH50 shows differences in Fe distributions between sampling times and slightly more oxidized conditions during the trades compared to the monsoon period, the seasonal variations are relatively subdued, with slightly lowered pore water Fe and solid phase oxidized Fe concentrations. The sediment was bioturbated at the GH50 foreset site, and no visual evidence of physical disturbance was obvious during seasonal sampling. Neither site has detectable dissolved sulfide. The monsoon distributions are comparable to those measured previously in the gulf [Aller et al., 2004; Alongi, 1995].

### 5.2.7. Remineralization Rates

[38] For the present purposes, the  $\Sigma\text{CO}_2$  net production rate distributions obtained from whole core incubations were integrated over the upper 0–20 cm and converted to equivalent areal  $\Sigma\text{CO}_2$  production fluxes using the measured sediment porosities (0.7–0.86). There were well defined spatial and seasonal differences in net  $\Sigma\text{CO}_2$  production fluxes (Figure 8). The highest values, ranging from  $\sim 30$  to  $42 \text{ mmol m}^{-2} \text{ d}^{-1}$ , were found during the monsoon periods at tidal channel and topset sites  $<35$  m, and the lowest, ranging from 3 to  $20 \text{ mmol m}^{-2} \text{ d}^{-1}$ , were measured at topset sites  $<35$  m during the late trades and

transition periods. With some exceptions, the production rates generally decreased seaward into the foreset and bottomset sites, and showed no evidence of seasonal variation at foreset site GH50. The magnitudes of the  $\Sigma\text{CO}_2$  production fluxes agreed well with previous measurements of  $\Sigma\text{CO}_2$  production rates and with estimates of benthic  $\text{O}_2$  fluxes, most of which were made during monsoon periods [Aller et al., 2004; Alongi, 1991, 1995; Alongi et al., 1993].

### 5.2.8. Pore Water $\Sigma\text{CO}_2$ and $\text{CH}_4$ Distributions and Isotopic Compositions

[39] Pore water concentrations of  $\Sigma\text{CO}_2$  increase substantially immediately below the sediment–water interface at all sites except GH75 (Figures 9–12), consistent with generally high remineralization rates and minimal bioturbation. The highest concentrations, reaching  $>40 \text{ mM}$  in the upper 1 m, are found in methanic zones below the episodically reworked layer on the topset. The lowest concentrations, 2–5 mM, are found at GH75 in the highly bioturbated bottomset deposits. A net decrease of  $\Sigma\text{CO}_2$  concentration within the underlying methanic zone is evident only at Purutu5 in the Fly delta plain, where total concentrations are relatively low ( $\sim 10 \text{ mM}$ ). As shown previously, pore waters throughout the gulf are at saturation or are supersaturated with respect to a range of common carbonate minerals below a thin surface zone of undersaturation which is usually much less than 10 cm [Aller et al., 2004].

[40] The  $\delta^{13}\text{C}$  of pore water  $\Sigma\text{CO}_2$  initially decreases with depth at all sites, reflecting metabolic inputs from remineralized  $\text{C}_{\text{org}}$ .  $\Sigma\text{CO}_2 \delta^{13}\text{C}$  reaches minimum basal values of  $-12\text{\textperthousand}$  on the bottomset,  $-21$  on the foreset,  $-25$  to  $-28\text{\textperthousand}$  on the topset, and  $-26\text{\textperthousand}$  in the mangrove channels.  $\Sigma\text{CO}_2$  becomes isotopically heavier in the deeper

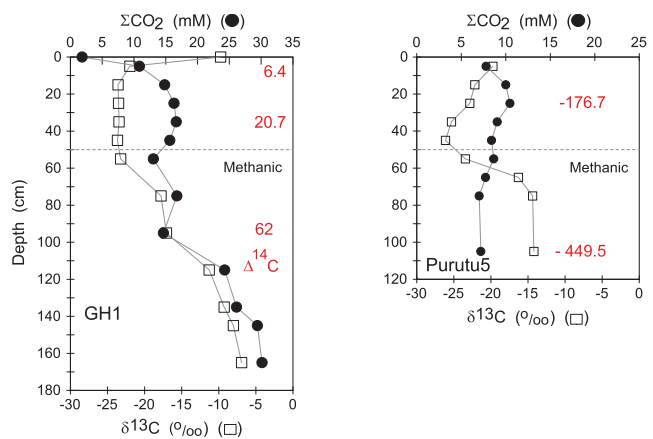


**Figure 9.** (left) Pore water  $\Sigma\text{CO}_2$  concentration (solid circles) and  $\Sigma\text{CO}_2 \delta^{13}\text{C}$  (open squares) profiles are shown from Wame River channel bar site GH1.  $\Sigma\text{CO}_2 \Delta^{14}\text{C}$  measured within discrete depth intervals are indicated as numbers down core. (right) Pore water  $\Sigma\text{CO}_2$  concentration (solid circles) and  $\Sigma\text{CO}_2 \delta^{13}\text{C}$  (open squares) profiles at Fly delta channel site Purutu5.  $\Sigma\text{CO}_2 \Delta^{14}\text{C}$  indicates remineralization of  $\text{C}_{\text{org}}$  aged 1560–4800 years in a deposit containing  $^{210}\text{Pb}_{\text{xs}}$  a few tens of meters from modern mangroves. In both cases, significant  $\Sigma\text{CO}_2$  concentrations and  $^{13}\text{C}$  enrichments are attained in the upper few centimeters. The  $\delta^{13}\text{C}$  increases substantially in the methanic zone.

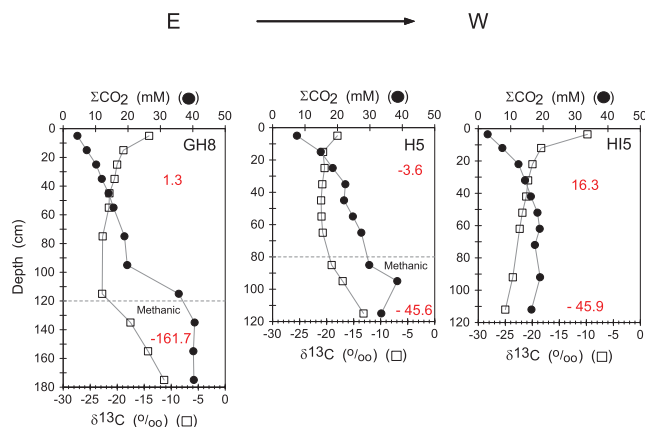


**Figure 10.** Pore water  $\Sigma\text{CO}_2$  concentration (solid circle) and  $\Sigma\text{CO}_2 \delta^{13}\text{C}$  (open squares) profiles at (left) GH8, (middle) H5, and (right) HI-5, represent an approximate along-isobath transect on the inner topset.  $\Sigma\text{CO}_2 \Delta^{14}\text{C}$  measured within discrete depth intervals are indicated as numbers down core. CH<sub>4</sub> was not evident in the sampled interval at HI-5. (Site H5 is the same as FF3 of Goñi *et al.* [2008].)

zones (>40–100 cm) at the mangrove channel and topset sites due to methanogenesis. The isotopic composition of CH<sub>4</sub> at topset site GH14 ( $\delta^{13}\text{C} = -81$  to  $-90$ ) is consistent with a biogenic source. CH<sub>4</sub> was not evident within the upper 7 m at foreset site GH50, as expected based on the presence of relatively high, constant concentrations of pore water SO<sub>4</sub><sup>2-</sup> at depth (Figure 7). At GS48 (HM50), CH<sub>4</sub> was present below 4.5 m at 0.10–0.83 mM with isotopic compositions  $-83$  to  $-90$  (not plotted).

[41] The  $\Delta^{14}\text{C}$  of pore water  $\Sigma\text{CO}_2$  in the upper few meters varied widely from +62 to  $-449.5\text{\textperthousand}$ . At most sites,  $\Sigma\text{CO}_2 \Delta^{14}\text{C}$  in the upper  $\sim 30$ –40 cm was  $>0$ , indicating the dominant decomposition of modern C<sub>org</sub> substrates formed since atmospheric testing of nuclear weapons ( $\sim 1960$ ). A significant exception is mangrove channel site

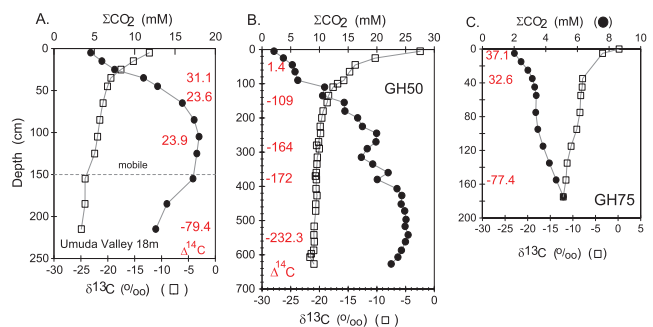


**Figure 12.** Pore water  $\Sigma\text{CO}_2$  concentration (solid circle) and  $\Sigma\text{CO}_2 \delta^{13}\text{C}$  (open squares) profiles are shown from (a) kasten core from Umuda Valley site T8-18 (18 m; mobile layer inferred from  $^{210}\text{Pb}_{xs}$  [Martin *et al.*, 2008] and solute profiles), (b) piston core from foreset site GH50, and (c) gravity core at bottomset site GH75. The  $\Sigma\text{CO}_2 \Delta^{14}\text{C}$  measured within discrete depth intervals are indicated as numbers down core.

Purutu5, where  $\Sigma\text{CO}_2 \Delta^{14}\text{C}$  is  $-176.7\text{\textperthousand}$  at  $\sim 30$  cm depth and reaches  $-449.5\text{\textperthousand}$  at 1 m, indicating remineralization of aged C<sub>org</sub> in migrating channel deposits. In contrast, at the mangrove channel bar site GH1, modern bomb signature  $^{14}\text{C}$  is released throughout the rapidly accumulating sediment pile ( $\sim 2$  m). Modern  $\Sigma\text{CO}_2 \Delta^{14}\text{C}$  also characterizes the mobile upper 1.5 m in the Umuda Valley, with substantial  $\Delta^{14}\text{C}$  decreases in deeper intervals. On the topset, there is a significant decrease of  $\Delta^{14}\text{C}$  in the methanic zone, reaching values  $<-150\text{\textperthousand}$  in the upper 1–2 m at sites along the GH transect. A similar decrease occurs in the non-methanic sediment of the foreset site GH50, and multiple other sites along the foreset (Figure 12) [Aller and Blair, 2004]. In the case of the foreset, however, depleted  $\Delta^{14}\text{C}$   $\Sigma\text{CO}_2$  is measured in steadily accreting deposits within intervals containing  $^{210}\text{Pb}_{xs}$ , whereas on the topset, the oldest  $\Delta^{14}\text{C}$  is measured beneath an erosional and diagenetic unconformity within zones lacking  $^{210}\text{Pb}_{xs}$  (Figures 3 and 11).

### 5.3. Net Reaction and Mixing Models

[42] Mixing models are used here to derive information on net changes and reactions associated with compositional variations in both solids and pore water during transport and diagenesis in the delta. Assuming multicomponent mixing between samples having concentrations, C<sub>j</sub>, of individual components with fixed property, P<sub>j</sub>, then the respective mass and property compositional balances for the mixture are given by

$$C_{\Sigma} = \sum_{j=1}^n C_j, \quad (1)$$

$$P_{\Sigma} C_{\Sigma} = \sum_{j=1}^n P_j C_j, \quad (2)$$

where total concentration and its integrated property composition are C<sub>Σ</sub> and P<sub>Σ</sub>, respectively, (e.g., bulk C<sub>org</sub> and δ<sup>13</sup>C). In these cases, the components are assumed

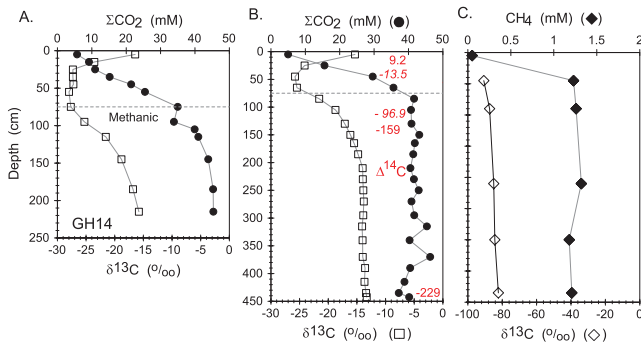


**Figure 11.** Pore water  $\Sigma\text{CO}_2$  concentration (solid circles) and  $\Sigma\text{CO}_2 \delta^{13}\text{C}$  (open squares) profiles from the middle topset site GH14: (a) kasten core and (b) piston core. The  $\Sigma\text{CO}_2 \Delta^{14}\text{C}$  measured within discrete depth intervals are indicated as numbers down core.  $\Delta^{14}\text{C}$  values in italics are from a gravity core sampled previously at the same site (HM13 [Aller and Blair, 2004]). (c) CH<sub>4</sub> concentrations (solid diamonds) and CH<sub>4</sub> δ<sup>13</sup>C (‰) (open diamonds) in the same piston core as Figure 11b.

normalized to a nonreactive constituent such as Al, or to total weight if nonconservative components are a relatively minor contribution. If progressive variation in concentration and property composition occurs from an initial mixture of reactants  $C_j(i)$ :

$$P_{\Sigma}C_{\Sigma} = \sum_{j=1}^n P_j C_j(i) + P_{\Delta}\Delta C_{\Sigma}. \quad (3)$$

In equation (3),  $\Delta C_{\Sigma}$  corresponds to the mass change in  $C_{\Sigma}$  from an initial condition ( $C_{\Sigma}(i) = \sum_{j=1}^n C_j(i)$ ), and  $P_{\Delta}$  defines its net value. For the case where there are net changes in the quantity  $C_{\Sigma}$ , ( $\Delta C_{\Sigma} \neq 0$ ), combining equations (1)–(3) gives

$$d(P_{\Sigma}C_{\Sigma})/dC_{\Sigma} = P_{\Delta} + (dP_{\Delta}/dC_{\Sigma})\Delta C_{\Sigma}, \quad (4)$$

$$P_{\Sigma} = \sum_{j=1}^n (P_j - P_{\Delta})/C_{\Sigma} + P_{\Delta}, \quad (5)$$

$$P_{\Delta} = \sum_{j=1}^n P_j [C_j - C_j(i)]/\Delta C_{\Sigma}. \quad (6)$$

Equation (4) demonstrates that the slopes of linear portions of a plot of  $P_{\Sigma}C_{\Sigma}$  versus  $C_{\Sigma}$  are direct estimates of the net change in bulk property  $P$  during progressive addition or removal processes [Sayles and Curry, 1988; Martin et al., 2000; Blair et al., 2003; Aller and Blair, 2006; Leithold et al., 2006]. For example, in a simple two-component isotopic composition model with terrestrial and marine end-members having fixed isotopic composition, the slope of a plot for  $\delta^{13}\text{C}^*C_{\text{org}}$  versus  $C_{\text{org}}$  reflects the net isotopic value of the  $C_{\text{org}}$  added or removed as terrestrial and marine contributions to bulk  $C_{\text{org}}$  vary. Alternatively, dividing both sides of equation (3) by  $C_{\Sigma}$  results in a linear relation between  $P_{\Sigma}$  and  $(1/C_{\Sigma})$  with intercept  $P_{\Delta}$  as  $(1/C_{\Sigma}) \rightarrow 0$  (equation (5)). As shown by equations (4) and (5), it is not necessary to know the number of contributing components in order to derive a value for the net property change  $P_{\Delta}$ , whereas equations (2) and (6) provide a means of interpreting specific contributions.

## 6. Discussion

### 6.1. Sources and Inputs of Sedimentary $C_{\text{org}}$

[43] The sedimentary  $C_{\text{org}}$  initially entering or produced within the Gulf of Papua is derived from multiple sources having widely varying metabolic reactivities. Typical river suspended matter and riverbed  $C_{\text{org}}$  concentrations within the lower reaches range between  $\sim 0.6$  and  $1.3 \text{ mmol g}^{-1}$  ( $0.75\text{--}1.5 \text{ wt \%}$ ; average  $1.1\%$ ) with bulk  $\delta^{13}\text{C}$  of  $-26.8\text{\textperthousand}$  (Fly) to  $-25.37\text{\textperthousand}$  (Wame-Purari), the latter isotopic value is based on a single sample (Table 2) [Bird et al., 1995; Keil et al., 1997; Brunskill et al., 2007b]. The total, individual river weighted flux of particulate  $C_{\text{org}}$  to the gulf is estimated to be  $152 \times 10^9 \text{ mol a}^{-1}$ , with an additional DOC flux of  $62 \times 10^9 \text{ mol a}^{-1}$  [Brunskill et al., 2007a].

Spread evenly over the clinoform area  $<50 \text{ m}$  depth ( $21.7 \times 10^9 \text{ m}^2$ ), this particulate terrestrial  $C_{\text{org}}$  flux corresponds to an average input of  $\sim 19 \text{ mmol C m}^{-2} \text{ d}^{-1}$ . If this flux were partitioned into the inner to mid topset ( $0\text{--}20 \text{ m}$ ;  $15.5 \times 10^9 \text{ m}^2$ ) and the outer topset-foreset ( $20\text{--}50 \text{ m}$ ;  $6.2 \times 10^9 \text{ m}^2$ ) on a basis simply proportional to the percentage of net accumulation of sediment in each region (34 and 66%), then respective inputs of  $9.1$  and  $44.3 \text{ mmol m}^{-2} \text{ d}^{-1}$  would be predicted. As shown subsequently, however, extensive modification of the river flux disproportionate to net accumulation patterns occurs during progressive transit and diagenetic processing on the energetic topset.

[44] The riverine  $C_{\text{org}}$  is a mixture of recycled rock kerogen, soil humus, vascular plant debris, and freshwater plankton [Blair et al., 2003; Goñi et al., 2008]. Given the mountainous, high-yield terrain (Fly and Purari,  $1\text{--}3 \text{ Kt km}^{-2} \text{ a}^{-1}$ ), kerogen is expected to contribute a portion of the  $C_{\text{org}}$ , possibly  $\sim 0.2\text{--}0.5 \text{ wt \%}$ , in the suspended sediment of this system [Komada et al., 2004; Blair et al., 2003; Leithold et al., 2006]. Aged soil humus derived from C3 vascular plants and modern C3 vascular plant debris dominates the remaining river particulate fractions [Bird et al., 1994; Goñi et al., 2006]. Suspended matter in five small rivers from eastern and northern Papua New Guinea averaged  $3.6 \pm 5.7\% C_{\text{org}}$  (median  $1.9\%$ ),  $\Delta^{14}\text{C} = -162 \pm 87$ ; and  $\delta^{13}\text{C} = -26.5 \pm 3.4$ , consistent with old soil  $C_{\text{org}}$  sources in at least a subset of rivers draining interior highlands [Raymond, 1999]. The bulk and mineral fraction  $C_{\text{org}}$  in surface deposits ( $0\text{--}0.5 \text{ m}$ ) seaward of the Fly River have  $\Delta^{14}\text{C}$  between  $-515$  and  $-644\text{\textperthousand}$ , perhaps reflecting the delivery of substantially aged, kerogen-rich debris, however, redistribution of older material within the delta or aging and reexposure in situ may also account for these values [Aller and Blair, 2004; Goñi et al., 2008].

[45] The initial suspended matter load is substantially augmented by inputs from mangrove and *Nypa* palm forests, and marine plankton production within the delta plain, resulting in concentrations for distributary channel surface suspended matter  $>10\% C_{\text{org}}$ , and creating a dramatic spatial halo of  $C_{\text{org}}$ -enriched, isotopically light ( $\delta^{13}\text{C} = -29$  to  $-30\text{\textperthousand}$ ) suspended particulates around the Fly delta plain distributary channel region [Robertson and Alongi, 1995; Robertson et al., 1998; Goñi et al., 2006]. Virtually all of the vascular plant  $C_{\text{org}}$  introduced to the particulate load within this region is remineralized in the proximal delta water column and in surfacemost sediment, with little incorporated into the seabed or reaching the central gulf topset. The process of loss and addition of  $C_{\text{org}}$  within this inshore zone and its average isotopic composition can be readily discerned from the mixing models outlined previously (equations (1)–(6)). A plot of  $\delta^{13}\text{C}^*C_{\text{org}}$  versus  $C_{\text{org}}$  for suspended matter in the Fly River distributary region and underlying surface seabed shows water column addition to the initial river suspended matter  $C_{\text{org}}$ , modest depletion of  $C_{\text{org}}$  in the surface seabed, and reveals that the dominant isotopic composition of the  $C_{\text{org}}$  added and lost in this region is  $-29.2\text{\textperthousand}$  (Figure 13). This net isotopic value is indicative of C3 mangrove and *Nypa* palm detritus and of a minor role for marine plankton [Cifuentes et al., 1996; Bouillon et al., 2003]. A comparable model plot for pore water  $\Sigma\text{CO}_2$  in the upper  $40 \text{ cm}$  at the Purutu5 mangrove channel site also implies remineralization of

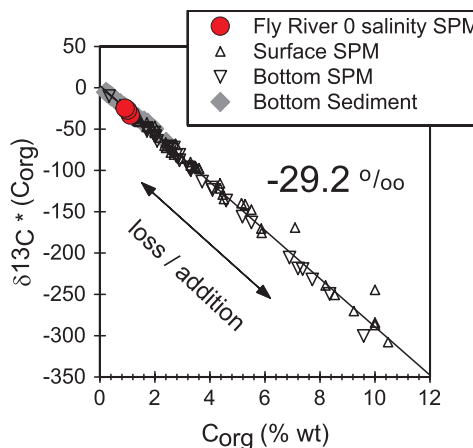


**Figure 13.** Addition and virtually immediate removal of sedimentary  $C_{org}$  in the Fly River delta plain distributary zone are demonstrated by a combined plot of  $C_{org}$  in initial Fly River suspended matter (0 salinity) (data from Keil *et al.* [1997] and Table 2 of this study), suspended matter in the surface and bottom water of the distributary channels, and the underlying surface seabed (0–1 cm) in the proximal Fly delta topset (data from Goñi *et al.* [2006]). The surface seabed generally shows modest depletion relative to suspended matter, which is substantially enriched within the delta plain. The net  $\delta^{13}\text{C}$  value of  $C_{org}$  added and removed in the process is  $-29.2\text{‰}$  (geometric mean slope), consistent with a dominant source from mangrove and *Nypa* palm vascular plant detritus derived from forests fringing the distributary channels, and with the  $\delta^{13}\text{C}$  of respiratory  $\Sigma\text{CO}_2$  released from channel sediments in the same region (Figures 9 (right) and 14).

substrate with a net isotopic value of  $-29.1\text{‰}$ , directly demonstrating the reactivity and remineralization of isotopically light  $C_{org}$  in delta plain channel deposits (Figure 14). The isotopic value of bulk  $C_{org}$  over large areas of the surface seabed in the proximal Fly delta averages  $\sim -26.3\text{‰}$  with  $C_{org} = 0.4\text{--}1.2\%$  [Goñi *et al.*, 2006], comparable to the initial Fly River suspended matter, and consistent with no substantial net addition and burial of mangrove forest detritus in offshore sediments. Thus the large introduction of reactive terrestrial C3 plant debris in the delta plain distributary channels and inshore mangrove forest regions is relatively transient and apparently has little net effect on the quantity of sedimentary  $C_{org}$  exported seaward to the deeper subaqueous delta topset and the central gulf.

[46] Net marine primary production occurs throughout the distributary channel and open shelf system, with measurements averaging  $\sim 4.3 \pm 2.5 \text{ mmol C m}^{-2} \text{ d}^{-1}$  in the Fly delta distributary region, and  $21 \pm 6$  to  $52.2 \pm 0.8 \text{ mmol C m}^{-2} \text{ d}^{-1}$  over the outer topset to bottomset region of the central gulf [Robertson *et al.*, 1998; McKinnon *et al.*, 2007]. The  $\delta^{13}\text{C}$  composition of this planktonic source has not been measured directly but is inferred to be  $-19.5$  to  $-20.5\text{‰}$ , based on measurements in the Great Barrier Reef to the south and on the inshore–offshore spatial patterns of bulk sediment  $C_{org}$  in the central Gulf of Papua [Bird *et al.*, 1995]. These net planktonic  $C_{org}$  production rates are either substantially less than or in the same range as the benthic remineralization fluxes measured seasonally across the gulf clinoform (Figure 8) [Aller *et al.*, 2004], implying the potential to consume the entire autochthonous planktonic production in underlying bottom waters and seabed. The lack of any substantial net buildup of isotopically heavy  $C_{org}$  in bottom sediments over the topset is consistent with

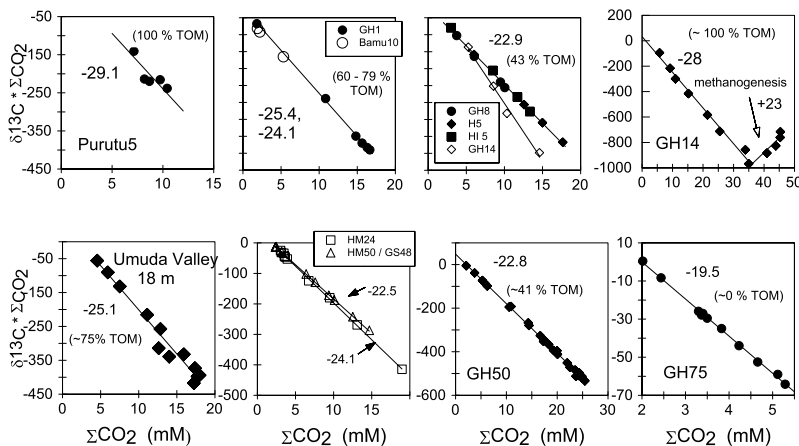


**Figure 14.** Pore water reaction model plots illustrate the net  $\delta^{13}\text{C}$  values (geometric mean slope) of  $\Sigma\text{CO}_2$  added over the modeled intervals. On the basis of assumed end-members of  $\leq -26.8$  and  $\geq -20\text{‰}$  for terrestrial and marine sources, respectively, the estimated% contribution of terrestrial  $C_{org}$  substrate ranges from 100 to 0% across the clinoform facies. The inshore distributary channel sites GH1 and Bamu10 show evidence of significant import of marine  $C_{org}$ , as do inner topset sites GH8, H5, and HI 5. The only site with no apparent contribution of light terrestrial  $C_{org}$  substrates is bottomset site GH75 ( $-19.5\text{‰}$ ). An average net addition of  $+23\text{‰}$  relative to an initial  $\Sigma\text{CO}_2$  pore water value of  $-26\text{‰}$  is shown in the upper region of the methanic zone at GH14. Note the nonlinear increase in the model slope (not fitted) as methanogenesis proceeds and light  $\text{CO}_2$  is progressively removed. (Standard error of slopes is 37% Purutu5 and  $2.3 \pm 1.9\%$  otherwise.)

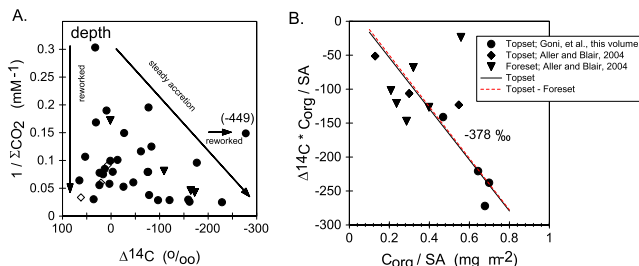


**Figure 15.** (a) Pore water  $\Sigma\text{CO}_2$  has a wide range of  $\Delta^{14}\text{C}$  in the upper 1–5 m of the clinoform, from more than modern to  $<-230\text{\textperthousand}$ . The relation of  $\Sigma\text{CO}_2$  concentration and  $\Sigma\text{CO}_2 \Delta^{14}\text{C}$  depends on the local depositional conditions, with reworked or rapidly deposited sediments such as GH1 (open diamonds) showing input of greater than modern  $^{14}\text{C}$  and little variation of  $\Delta^{14}\text{C}$  as  $\Sigma\text{CO}_2$  increases, while steadily accreting deposits such as GH50 (solid triangles) show substantial input of ancient  $\Sigma\text{CO}_2$  (e.g., intercept value  $>-250\text{\textperthousand}$ ; model equation (5)). (b) As shown by the slopes of plots of  $\Delta^{14}\text{C} * \text{C}_{\text{org}}/\text{SA}$  versus  $\text{C}_{\text{org}}/\text{SA}$  for either the topset sites alone or topset-foreset sites combined, in addition to the obvious rapid respiratory loss of young  $\text{C}_{\text{org}}$  substrates into pore and overlying water. There is a slow net loss of ancient  $\text{C}_{\text{org}}$  (average age  $\sim 4000$  years) as sediment moves across the clinoform facies and the overall  $\text{C}_{\text{org}}$  loading decreases (see also Figure 19; data from Aller and Blair [2004] and Goñi et al. [2008]). (Standard errors of slopes are 13% topset and 16% topset-foreset.)

complete remineralization of marine planktonic sources in this region (Table 2) [Bird et al., 1995; Aller and Blair, 2004; Goñi et al., 2008].

## 6.2. Sources of Remineralized $\Sigma\text{CO}_2$

[47] Mixing model evaluation of pore water  $\Sigma\text{CO}_2$  and isotopic distributions demonstrate that a broad range of  $\text{C}_{\text{org}}$  substrates from multiple sources are decomposed across the clinoform facies. The net isotopic values of decomposing substrates range from a minimum of  $-29.1\text{\textperthousand}$  in the Purutu Island mangrove channel to  $-19.5\text{\textperthousand}$  in the bottomset (GH75) (Figure 14). Anaerobic oxidation of  $\text{CH}_4$  and carbonate mineral precipitation may contribute to these calculated values in some cases, making them possible minimum estimates [e.g., Sivan et al., 2002]. However, anaerobic oxidation of  $\text{CH}_4$  is unlikely to be significant except in restricted intervals similar to those at topset site GH14 (Figures 6 and 11), and early diagenetic carbonate mineral precipitation is of minor importance in gulf sediments over the depth zones considered [Aller et al., 2004; T. Fang et al., manuscript in preparation, 2007]. The deeper methanic zones are characterized by a net input of heavy  $\Sigma\text{CO}_2$ , reflecting removal of light  $\text{CO}_2$  during methanogenesis (e.g., at GH14, net addition of  $\sim +23$  relative to  $-26\text{\textperthousand}$   $\Sigma\text{CO}_2$  pool; Figure 14).

[48] The fact that both the inshore Bamu and Wame River channel deposits, surrounded by mangroves and *Nypa* palm forests, release relatively heavy  $\Sigma\text{CO}_2$ ,  $-24$  to  $-25.4\text{\textperthousand}$ , implies the availability of reactive marine planktonic substrates within the mangrove distributary channel facies. The

importation of marine planktonic debris from the topset into the mangrove distributary channels is consistent with cross-shelf particle exchange during estuarine flow and with the unusually high  $^{210}\text{Pb}_{\text{xs}}$  activities at GH1 (Figure 4). River suspended matter normally has  $^{210}\text{Pb}_{\text{xs}} < 10\text{--}20 \text{ Bq kg}^{-1}$ , indicating import of  $^{210}\text{Pb}_{\text{xs}}$  tagged particles from the shelf [Brunskill et al., 2007b; Aalto et al., 2008]. With exceptions such as GH14, many inner-outer topset sites are remineralizing  $\text{C}_{\text{org}}$  with a net isotopic composition between  $-22.9$  and  $-24.1\text{\textperthousand}$ , increasing progressively to  $-22.0$  to  $-23.0\text{\textperthousand}$  on the foreset. The net isotopic value of remineralized  $\Sigma\text{CO}_2$  in the Umuda Valley is  $-25.1\text{\textperthousand}$ , implying a primarily terrestrial  $\text{C}_{\text{org}}$  metabolic source in these highly mobile sediments.

[49] Approximate estimates of the relative contributions of terrestrial and marine sources to diagenetic remineralization can be made assuming simple two-component mixing between terrestrial and marine end-members having average isotopic values of  $\leq -26.8 \pm 0.5\text{\textperthousand}$  and  $\geq -20 \pm 0.5\text{\textperthousand}$ , respectively. The contributions of terrestrial organic matter to remineralization range from 100% inshore to 0% offshore, with most topset and foreset sites  $\sim 40\%$ ; decreasing to  $\sim 35\%$  if a terrestrial end-member of  $-28\text{\textperthousand}$  is assumed (Figure 14). These estimates demonstrate that marine  $\text{C}_{\text{org}}$  dominates early diagenetic remineralization at many sites but that except at the deepest bottomset sites, terrestrial  $\text{C}_{\text{org}}$  components are a significant, sometimes major, proportion of the decomposing substrate throughout the subaqueous clinoform (topset–Umuda Valley average =  $61 \pm 26\%$  terrestrial). Assuming seasonally averaged benthic  $\Sigma\text{CO}_2$  production rates of  $\sim 24 \pm 10 \text{ mmol m}^{-2} \text{ d}^{-1}$  in the upper 20 cm of the topset (Figure 8; time weighting values 2/3 monsoon; 1/3 trades and transition), these percentages indicate a terrestrially sourced benthic  $\text{C}_{\text{org}}$  remineralization rate  $\sim 15 \pm 6 \text{ mmol m}^{-2} \text{ d}^{-1}$ . The increased abundance of Chl *a* in surface sediment during the monsoons relative to the trades suggests that much of the seasonal excursions in remineralization rates are related to inputs of labile marine  $\text{C}_{\text{org}}$  [Aller et al., 2008].

## 6.3. Ages and Reactivity of Decomposing Sedimentary $\text{C}_{\text{org}}$

[50] The wide range of terrestrial and marine  $\text{C}_{\text{org}}$  substrates decomposed during early diagenesis in the upper few meters across the clinoform facies also have a broad spectrum of ages, as shown by  $\Sigma\text{CO}_2$  with  $\Delta^{14}\text{C}$  ranging from  $>0$  (modern) in the surface 40 cm at most sites, to  $-229\text{\textperthousand}$  (2030 years) at depth in the topset and foreset. The inshore mangrove channels show the widest variation in  $\Sigma\text{CO}_2$  ages with  $>\text{modern}$  in the Wame channel bar and  $\sim 1600$  to 4800 years in Purutu channel sediments (Figure 9), the latter presumably reflecting channel migration and undercutting of old deposits. The relationships between  $\Delta^{14}\text{C}$  and  $\Sigma\text{CO}_2$  are determined largely by local depositional environment, with rapidly deposited sediment often characterized by  $\Delta^{14}\text{C} > 0$  across all ranges of  $\Sigma\text{CO}_2$ , and steadily accumulating deposits on the foreset characterized by regular inverse relationships between  $\Delta^{14}\text{C}$  and  $\Sigma\text{CO}_2$  (Figure 15). Sediment  $\text{C}_{\text{org}}$  also directly shows evidence for net loss of old components having a mean  $\Delta^{14}\text{C}$  of  $-378\text{\textperthousand}$  (3926 years), with much of the removal on the topset (Figure 15). These

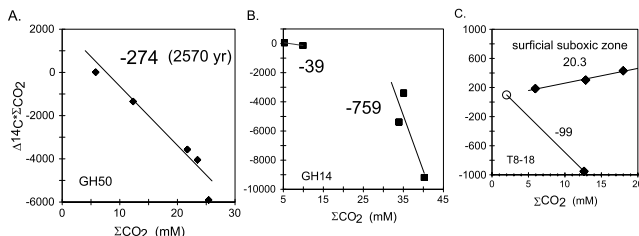


**Figure 16.** (a) Net  $\Delta^{14}\text{C}$  value of  $\Sigma\text{CO}_2$  added to pore water in the  $\text{SO}_4^{2-}$  reduction zone below  $\sim 0.5$  m at foreset site GH50 is  $-274\text{\textperthousand}$ , implying virtually complete absence of young labile components in material delivered to the foreset (or less likely, mixing of much older  $\Sigma\text{CO}_2$  to a labile pool). (b) Net  $\Delta^{14}\text{C}$  of  $\Sigma\text{CO}_2$  in the surface mobile zone at GH14 is  $-39\text{\textperthousand}$ , essentially modern, whereas in the underlying relict methanic deposits the net value is  $-759\text{\textperthousand}$ . This latter extremely depleted value, which is smaller than any measured bulk  $\text{C}_{\text{org}}$  in the upper 2 m at topset sites, implies the remineralization of kerogen, carbonate precipitation, substantially aged sediment below  $\sim 2$  m, or the transport (diffusion upward) of  $^{14}\text{C}$  depleted  $\Sigma\text{CO}_2$  into this zone. (c) Surface  $\sim 1.5$  m of suboxic sediment in the Umuda Valley remineralizing modern  $\text{C}_{\text{org}}$  substrate ( $\Delta^{14}\text{C} = +20.3\text{\textperthousand}$ ). Extrapolation of a single  $\Delta^{14}\text{C}$  value in the underlying deposit to a likely initial value in overlying water (open circle), implies a distinctly different, older source ( $-99\text{\textperthousand}$ ) and a likely depositional unconformity.

mean values presumably reflect mixtures of metabolic substrates with widely varying ages.

[51] Relatively old  $\text{C}_{\text{org}}$  is clearly also decomposing in the rapidly accumulating foreset facies, as demonstrated by a plot of  $\Delta^{14}\text{C}$   $\Sigma\text{CO}_2$  versus  $\Sigma\text{CO}_2$  from 0.5–6 m depth at GH50, which indicates net release of  $\Sigma\text{CO}_2$  exceeding a 2500 year conventional  $^{14}\text{C}$  age ( $\sim 2100$  years,  $\Delta^{14}\text{C} = -230\text{\textperthousand}$ , in the upper 0.5–4 m). As shown by the  $^{210}\text{Pb}_{\text{xs}}$  distribution and sediment accumulation rate at this site ( $1.7 \text{ cm a}^{-1}$ ), the remineralization of ancient  $\text{C}_{\text{org}}$  is occurring in sediment deposited within the last 100–200 years (Figure 16). Similarly old  $\Sigma\text{CO}_2$  is released in the upper 2–3 m throughout the rapidly deposited foreset region [Aller and Blair, 2004]. This fact shows that old  $\text{C}_{\text{org}}$  is remineralized in the  $\text{SO}_4^{2-}$  reduction zone during steady accretion (Figure 6) and is consistent with the observed solid-phase losses (Figure 15). It further implies that remineralization of aged pools must occur at a slow rate continuously in other clinoform facies and during the process of sediment transport through oxygenated waters to the foreset [e.g., Keil et al., 2004; Ogston et al., 2008]. The remineralization of aged  $\text{C}_{\text{org}}$  ( $\Sigma\text{CO}_2 \sim 1600$  years) in migrating mangrove channel deposits containing excess  $^{210}\text{Pb}$  (Purutu5, Figures 4 and 9), also supports the concept of continuous loss of refractory components during particle transport from source to sink.

[52] The reactivity of the decomposing  $\text{C}_{\text{org}}$  pool on the foreset can be estimated from the  $\text{SO}_4^{2-}$  pore water distributions below the bioturbated zone by assuming steady accumulation, no compaction, and a single reactive  $\text{C}_{\text{org}}$  pool over the interval of interest [Berner, 1980]. The attenuation of the  $\text{SO}_4^{2-}$  profiles with depth is determined in this case by the ratio  $k/\omega$ , with  $k$  = reaction rate constant

and  $\omega$  = sediment accumulation rate. Excellent fits of this classic diagenetic model in zones below the bioturbated zone are obtained in piston cores at both GH50 and GS48 ( $\text{SO}_4^{2-}$  data not shown), resulting in  $k/\omega = 0.0084$  and  $0.0052 \text{ cm}^{-1}$ , respectively (Figure 6). Given the measured accumulation rates,  $k$  equals  $0.014 \text{ a}^{-1}$  and  $0.019 \text{ a}^{-1}$  at GH50 and GS48, which are 10 to 15 times lower than predicted based on nondeltaic correlations between  $k$  and  $\omega$  [Toth and Lerman, 1977; Tromp et al., 1995]. These low reactivities demonstrate that the sedimentary  $\text{C}_{\text{org}}$  delivered to the foreset from the topset is relatively depleted in reactive components, as also shown previously by initial  $\text{SO}_4^{2-}$  concentration gradient modeling at additional foreset sites [Aller et al., 2004]. The initial decomposition rates measured in the foreset region ( $\Sigma\text{CO}_2 \sim 20 \text{ mmol m}^{-2} \text{ d}^{-1}$ ) must therefore be sustained by a relatively small quantity of reactive, marine organic matter that is largely decomposed within the bioturbated zone (Figures 6, 8, and 12).

[53] Topset sites and the Umuda Valley are characterized by a reworked, suboxic surface layer of variable extent, generally  $\sim 10$ –30 cm thick over much of the topset and up to  $\sim 150$  cm in the Umuda Valley (Figure 12;  $\text{Fe}^{2+}$  profiles (data not shown)) ( $^{210}\text{Pb}_{\text{xs}}$  [Martin et al., 2008]). As noted previously, the  $\Sigma\text{CO}_2$  being released in this mobile suboxic zone is generally modern ( $\Delta^{14}\text{C} > 0$ ), although older material is also clearly degraded but is not a dominant source. For example, at least during some periods, the surface zone at GH14 is characterized by net input of  $\Sigma\text{CO}_2$  with  $\Delta^{14}\text{C}$  of  $-39$  ( $\sim 330$  years) (Figure 16). At H5 (equivalent to station FF3 of Goñi et al. [2008]), a  $\Sigma\text{CO}_2 \Delta^{14}\text{C} = -3.6\text{\textperthousand}$  at 20–30 cm implies net input of  $\Sigma\text{CO}_2$  with  $\Delta^{14}\text{C} \sim -12\text{\textperthousand}$ , if an initial overlying water value of  $+67\text{\textperthousand}$  is assumed for the topset region [Aller and Blair, 2004]. Unlike the foreset, however, sites with a surface reworked zone show a large, discontinuous change in the age of  $\Sigma\text{CO}_2$  introduced below the reworked layer, consistent with a depositional and diagenetic unconformity between the suboxic layer and the underlying, often methanic, deposit. The net addition of  $\Sigma\text{CO}_2$  with extremely depleted  $\Delta^{14}\text{C}$  ( $-759\text{\textperthousand}$ ) below 40 cm at GH14 implies that either ancient kerogen-like  $\text{C}_{\text{org}}$  is being remineralized locally or, more likely, that  $^{14}\text{C}$ -depleted  $\Sigma\text{CO}_2$  is diffusing upward from deeper deposits. Removal of  $\text{CO}_2$  by carbonate precipitation without isotopic fractionation would minimize the net  $\Delta^{14}\text{C}$  of added  $\Sigma\text{CO}_2$ .

#### 6.4. Diagenetic Fractionation

[54] Although a broad spectrum of sedimentary  $\text{C}_{\text{org}}$  is remineralized in the water column and seabed throughout the clinoform, at many sites there is preferential remineralization of marine relative to terrestrial  $\text{C}_{\text{org}}$ , and young relative to old  $\text{C}_{\text{org}}$ , consistent with observations in numerous soil and water column studies [Trumbore and Zheng, 1996; McCallister et al., 2004; Blair et al., 2003; Raymond and Bauer, 2001]. Comparison of  $\delta^{13}\text{C}$  in diagenetically released  $\Sigma\text{CO}_2$  to the associated bulk  $\text{C}_{\text{org}}$  demonstrates that, metabolically  $\Sigma\text{CO}_2$  released in the upper 0.5–1 m is often preferentially enriched in  $^{13}\text{C}$  by 1–4‰ (Figure 17a). This enrichment is consistent with the presence of a relatively small quantity of marine planktonic  $\text{C}_{\text{org}}$  sufficient to dominate early diagenetic remineralization and the initial production rates of  $\Sigma\text{CO}_2$ , but which is not abundant

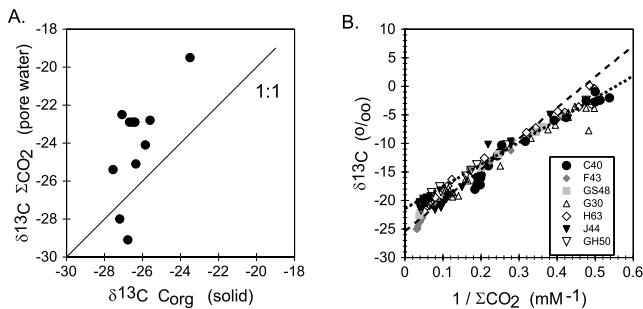


**Figure 17.** (a) Comparison of the net  $\delta^{13}\text{C}$  value of released  $\Sigma\text{CO}_2$  (Figure 14) with  $\delta^{13}\text{C}$  of  $\text{C}_{\text{org}}$  at the same site demonstrates a typical diagenetic fractionation of 1–4‰, consistent with previous findings of Aller and Blair [2004]. Exceptions occur when abundant labile vascular plant detritus is present, such as at distributary channel site Purutu5 and, presumably, middle topset site GH14. (b) Curvilinear nature of a plot of  $1/\Sigma\text{CO}_2$  in pore water versus its  $\delta^{13}\text{C}$  value on the foreset (see locations in Figure 1) demonstrates preferential release of marine relative to terrestrial-sourced  $\Sigma\text{CO}_2$ , as  $\Sigma\text{CO}_2$  increases. For  $1/\Sigma\text{CO}_2 > 0.25$ , the intercept of the tangent is  $-21.4\text{\textperthousand}$ , whereas for  $1/\Sigma\text{CO}_2 < 0.25$  the intercept is  $-25.4\text{\textperthousand}$  (see equation (5)) (data at sites other than GH50 from T. Fang et al. (manuscript in preparation, 2007)).

enough to strongly influence bulk  $\text{C}_{\text{org}}$  isotopic compositions at most sites, nor to be preserved [Aller and Blair, 2004]. As shown by the earlier diagenetic model estimates of  $\text{C}_{\text{org}}$  reactivity in the foreset and by the bulk isotopic values of sedimentary  $\text{C}_{\text{org}}$  across the topset, this relatively heavy (isotopically), reactive pool is lost within either the physically or biologically reworked surface zones.

[55] A compilation of  $\Sigma\text{CO}_2$  concentrations and isotopic analyses obtained over the upper 3–6 m on the outer topset

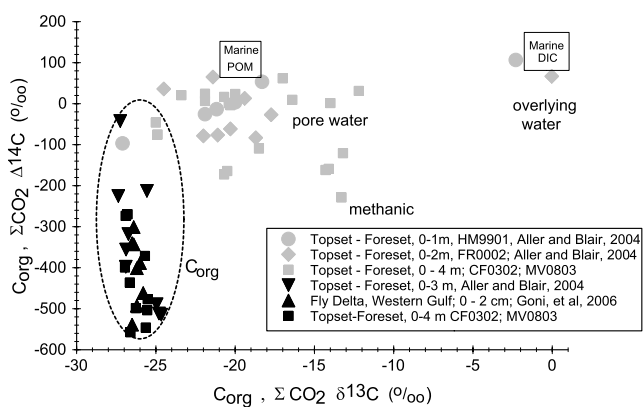


**Figure 18.** Relationships between both  $\Delta^{14}\text{C}$  and  $\delta^{13}\text{C}$  in the solid phase  $\text{C}_{\text{org}}$  and respiratory  $\Sigma\text{CO}_2$  in pore water demonstrate that diagenetic fractionation is common. In general, young substrates are utilized preferentially to older substrates and marine (heavy) relative to terrestrial (light). (Data were summarized from this study, Aller and Blair [2004], and Goñi et al. [2006].) The marine particulate organic matter and dissolved inorganic carbon fields are based on the work by Druffel et al. [2001, 2005].

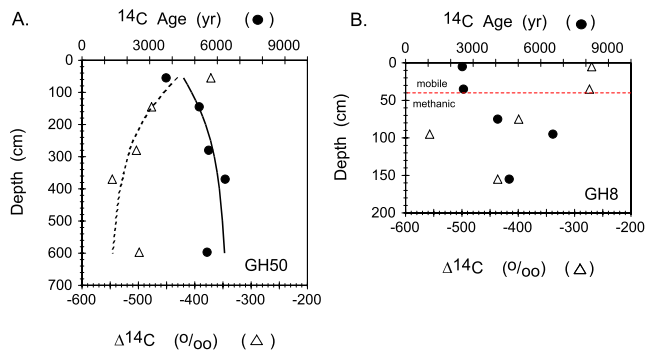


**Figure 19.** (a) Vertical profile of  $\text{C}_{\text{org}} \Delta^{14}\text{C}$  (open triangles) and corresponding conventional  $^{14}\text{C}$  age (solid circles) distributions at GH50 are consistent with apparent aging during diagenesis. The initial activity gradient (0–4 m) implies an accumulation rate of  $0.12 \text{ cm a}^{-1}$ ,  $\sim 15$  times lower than the  $^{210}\text{Pb}_{\text{xs}}$  profile over the same interval (Figure 4). The model curves represent the predicted profiles in the case where a reactive pool ( $\text{C}_{\text{org}} = 0.32 \text{ mmol g}^{-1}$ ;  $k = 0.014 \text{ a}^{-1}$ ) with a time-averaged  $\Delta^{14}\text{C}$  of  $-230\text{\textperthousand}$  is lost from the solid during remineralization assuming an accumulation rate of  $1.7 \text{ cm a}^{-1}$ . Both the reactive and nonreactive pools age by  $\Delta^{14}\text{C} \sim -18\text{\textperthousand}$  due to radioactive decay during the burial period, whereas the total  $\text{C}_{\text{org}}$  pool changes by  $\sim -115\text{\textperthousand}$  due to diagenetic loss of the reactive portion. (b) Two-zone diagenetic regime typical of the topset expressed in the  $\text{C}_{\text{org}} \Delta^{14}\text{C}$  distribution at GH8 (inner topset;  $^{210}\text{Pb}_{\text{xs}}$  homogeneous 0–40 cm). The stepwise change in ages ( $\sim 1500$  years) at the zonal boundary is consistent with a depositional unconformity. The age of the material in the surface zone is comparable to surface sediment on the foreset, reflecting the role of topset as source.

and foreset in this and earlier studies demonstrates that as a general rule diagenetic  $\Sigma\text{CO}_2$  becomes progressively lighter with burial depth. The initial compositional changes are characterized by an average net input of  $\Sigma\text{CO}_2$  with  $\delta^{13}\text{C} = -21.4$  grading to an average of  $-25.4\text{\textperthousand}$  (Figure 17b). These patterns imply early diagenetic loss of relatively reactive marine substrates and continued decomposition of residual refractory  $\text{C}_{\text{org}}$ , the latter dominated by old terrestrial sources. In the case of  $^{14}\text{C}$ , similar depth-dependent relative discrimination patterns occur with respect to substrate age: Typical enrichments of  $\Sigma\text{CO}_2 \Delta^{14}\text{C}$  compared to the solid phase are  $\sim 300\text{\textperthousand}$  or greater (Figure 18) [Aller and Blair, 2004]. It is clear, however, that despite time-dependent preferential reaction, virtually every component of sedimentary  $\text{C}_{\text{org}}$  is eventually subject to decomposition.

## 6.5. Bulk $^{14}\text{C}_{\text{org}}$ and Diagenetic Aging

[56] Diagenetic fractionation can result in the apparent aging of the bulk  $\text{C}_{\text{org}}$  independently of radioactive decay. Assuming steady initial activities of  $^{14}\text{C}$ , vertical profiles of  $\text{C}_{\text{org}} \Delta^{14}\text{C}$  on the foreset show a far more rapid change in  $^{14}\text{C}$  age with depth than predicted on the basis of  $^{210}\text{Pb}_{\text{xs}}$  distributions at the same sites [Aller and Blair, 2004]. In the case of GH50, where a well resolved  $^{14}\text{C}$  profile is available for example, the  $^{14}\text{C}$  predicted accumulation rate is  $\sim 0.12 \text{ cm a}^{-1}$  compared to a  $^{210}\text{Pb}_{\text{xs}}$ -determined rate of  $1.7 \text{ cm a}^{-1}$  (Figures 19 and 4). Time-dependent forms of the

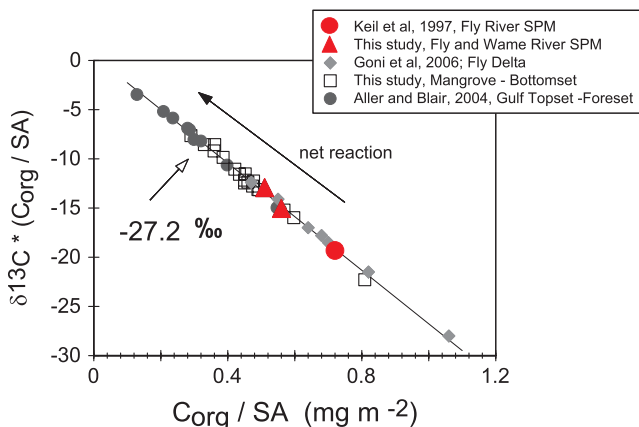


**Figure 20.** With the exception of the distributary channel delta plain regions where transient introduction of reactive vascular plant  $C_{org}$  occurs (Figure 13), deposits in the Gulf of Papua generally become progressively depleted in  $C_{org}$  relative to initial river suspended matter. The net isotopic value of the  $C_{org}$  removed is  $-27.2\text{\textperthousand}$ , consistent with a dominant net loss of terrestrial  $C_{org}$  without substantial replacement by marine  $C_{org}$  in the region examined. The various  $\Delta^{14}\text{C}$  and  $\delta^{13}\text{C}$  relationships between  $\Sigma\text{CO}_2$  and  $C_{org}$  demonstrate that  $C_{org}$  of virtually all ages and sources is remineralized at a wide range of rates, although relatively young  $C_{org}$  substrates dominate  $\Sigma\text{CO}_2$  production at any given time (Figures 15–18).

mass balance equations (1)–(2) can be used to estimate  $^{14}\text{C}$  activity profiles consistent with differential diagenetic remineralization of  $C_{org}$  pools of varying age over finite depth intervals. Assuming that over a restricted depth interval a single reactive  $C_{org}$  pool ( $dC_{org(j)}/dt = -k_j C_{org(j)}$ ) and a nonreactive pool ( $k = 0$ ) are present, each with a  $\Delta^{14}\text{C}_j$  value changing with time only as a function of radioactive decay, then vertical profiles of total  $C_{org}(t)$  and total  $\Delta^{14}\text{C}(t)$  can be calculated as a function of both reactive pool remineralization and radioactive decay in all pools. Model profiles for the case when a reactive pool is lost with a time averaged  $\Delta^{14}\text{C} = -230\text{\textperthousand}$ ; are shown in Figure 19, assuming an accumulation rate of  $1.7 \text{ cm a}^{-1}$ , a decomposing  $C_{org}$  pool ( $0.32 \text{ mmol g}^{-1}$ ) with first-order reaction rate constant  $k = 0.014 \text{ a}^{-1}$  (obtained from  $\text{SO}_4^{2-}$  profile model (Figure 6, right); also comparable to the rate constant estimated directly from the total  $C_{org}$  profile,  $k = 0.019 \text{ a}^{-1}$  (Figure 5)), and a relatively unreactive  $C_{org}$  pool ( $0.67 \text{ mmol g}^{-1}$ ) over the same interval with a terminal  $\Delta^{14}\text{C} = -546\text{\textperthousand}$  at 4 m. In addition to being consistent with the phenomenon of diagenetic aging, these model profiles also illustrate the agreement between processes implied by both pore water ( $\text{SO}_4^{2-}$ ,  $\Sigma\text{CO}_2$ ,  $\Delta^{14}\text{C}$ ) and solid phase data when steady accumulation occurs.

[57] Although diagenetic aging must occur continuously during remineralization throughout the deltaic system, depositional conditions do not allow its expression in progressive vertical changes of  $C_{org}$   $\Delta^{14}\text{C}$  except in cases of regular accumulation such as occur on the foreset. In contrast to the foreset,  $C_{org}$   $\Delta^{14}\text{C}$  profiles on the topset reflect the two-layer diagenetic regime typical of that facies: a mobile surface, batch reactor layer unconformably overlying dia-

genetically distinct, stable deposits (Figure 19b). The conventional  $^{14}\text{C}$  age of bulk  $C_{org}$  in the suboxic surface zone at inner topset site GH8,  $\sim 2500$  years, averages  $\sim 1500$  years younger than in the more consolidated underlying methanic deposits ( $>4000$  years). The stepwise transition in ages reflects the depositional discontinuity. The  $^{14}\text{C}$  age of bulk  $C_{org}$  in the topset mobile layer is comparable to that commonly found in the upper 0.5 m on the foreset, consistent with the initial processing of sediment on the topset and its progressive movement seaward.

## 6.6. $C_{org}$ Incineration and Burial

[58] The spatial patterns of  $C_{org}$  loading and progressive changes in the bulk isotopic composition of  $C_{org}$  across the topset-bottomset facies (shift from  $\leq -26.8$  to  $\geq -23.5\text{\textperthousand}$ ) demonstrate an overall net loss of terrestrial  $C_{org}$  within these central gulf regions relative to initial riverine suspended matter (Figure 20) [Bird et al., 1995; Aller and Blair, 2004; Goñi et al., 2008]. The net stable isotopic value of the lost sedimentary  $C_{org}$  averages  $-27.2\text{\textperthousand}$ , consistent with removal of terrestrially sourced  $C_{org}$  (Figure 20). As shown earlier, the large flux to the seabed of modern vascular plant debris in the delta plain distributary channels is transient and essentially eliminated within its area of input (Figure 13) [Robertson et al., 1998; Goñi et al., 2006]. The lack of major shifts in bulk sediment isotopic composition over large areas of the inner and middle topset of the central gulf ( $-27.2$  to  $-26.4\text{\textperthousand}$ ) (Table 3) [Bird et al., 1995; Goñi et al., 2008] also confirms that fresh marine plankton introduced to that region, which supports 25–60% of the early diagenetic  $\Sigma\text{CO}_2$  production, is largely remineralized, leaving little or no record in the seabed organic phase. Of course, the balances between governing processes, sources, and specific reactions of sedimentary material may vary in other subregions of the system such as southwest of the Fly or within the shelf valleys [Goñi et al., 2008; Martin et al., 2008].

[59] The measured benthic remineralization rates, which are minima because only the upper 20-cm layer is considered and because incubation methodology minimizes rates, are nevertheless sufficiently high relative to the inputs of material to account for loss of a substantial proportion of the terrestrial sedimentary  $C_{org}$  delivered to the gulf. As shown earlier, remineralization rates on the inner midtopset (0–20 m) have an approximate weighted seasonal average of  $\sim 24 \pm 10 \text{ mmol m}^{-2} \text{ d}^{-1}$  (assuming 2/3 monsoon, 1/3 trades and transition seasonal weighting), of which  $\sim 15 \pm 6 \text{ mmol m}^{-2} \text{ d}^{-1}$  is derived from terrestrial sources (Figures 8 and 12; assuming simple average% terrestrial at stations  $<20$  m). In comparison, if the river particulate  $C_{org}$  flux were initially focused entirely onto the inner–midtopset region ( $15.5 \times 10^9 \text{ m}^2$ ), then the input flux to that area is  $26.9 \text{ mmol m}^{-2} \text{ d}^{-1}$ . Thus, although it is not the primary clinoform depocenter, the inner–midtopset alone remineralizes  $\sim 56\%$  of the entire riverine particulate  $C_{org}$  flux on a steady basis as sediment transits and is refluxed within this region.

[60] Because of physical reworking, net accumulation rates of sediment on the inner midtopset are uncertain, whereas accumulation rates measured within the outer topset (20–30 m) and foreset (30–50 m) are far better constrained (e.g., Figure 4) [Brunskill et al., 2003; Walsh et al., 2004]. The outer topset and foreset store  $24.4 \times 10^9$  and

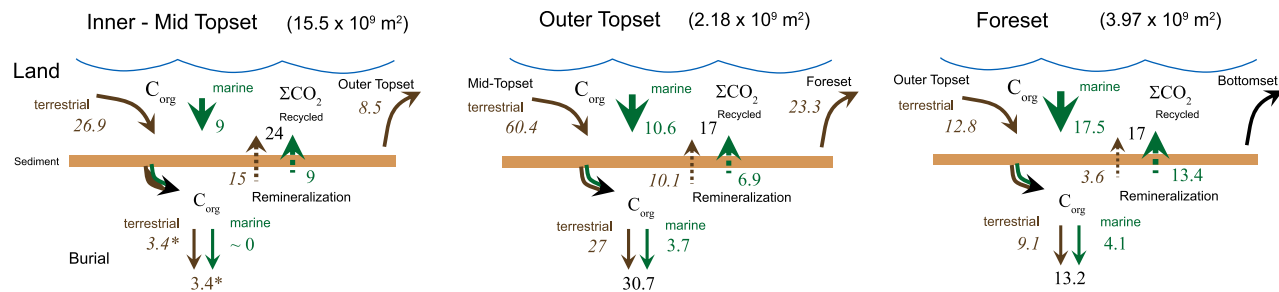


**Figure 21.** Approximate diagenetic  $C_{org}$  budgets on the topset and foreset were estimated assuming progressive movement of sediment from the inner topset to the foreset regions and successive areal focusing of residual material (terrestrial component in italics). The burial rate of  $C_{org}$  on the topset was determined by the difference between the initial river supply to the gulf, the burial rates in the outer topset and foreset, and the estimated remineralization rates in each facies. The marine inputs to the seabed were estimated from the seasonally averaged remineralization rates (Figure 8) and the average percent terrestrial  $\Sigma CO_2$  released at the sampling sites in each region (Figure 14). The marine input to the seabed varies substantially seasonally, and the values used are conservative. These budgets, although approximate, demonstrate the central role of the topset in remineralizing  $C_{org}$ , which oxidizes >50% of the river input while storing ~13–27%. The budget units are  $mmol\ C_{org}\ m^{-2}\ d^{-1}$ . The areas of the inner midtopset, outer topset, and foreset regions are  $15.5$ ,  $2.18$ , and  $3.97 \times 10^9\ m^2$ , respectively [Brunskill et al., 2003].

$19.1 \times 10^9\ mol\ C_{org}\ a^{-1}$ , respectively, or  $30.7$  and  $13.2\ mmol\ C_{org}\ m^{-2}\ d^{-1}$  on an areal basis; assuming mean accumulation rates of  $18.5$  and  $9.6\ kg\ m^{-2}\ a^{-1}$  and areas of  $2.18$  and  $3.97 \times 10^9\ m^2$  [Brunskill et al., 2007a, 2007b]. On the basis of  $\delta^{13}C$  distributions, virtually all of the  $C_{org}$  buried on the inner midtopset is of terrestrial origin, ~88% is terrestrial on the outer topset and ~69% on the foreset (assuming mean values of  $-26$  and  $-24.7 \pm 1.9\ \text{‰}$  on the outer topset and foreset, respectively, and terrestrial-marine end-members  $-26.8$  and  $-20\ \text{‰}$  [Bird et al., 1995; Aller and Blair, 2004; Goñi et al., 2008]). By adding the measured burial fluxes from the outer topset and foreset together with the annual average  $\Sigma CO_2$  remineralization rate fluxes in the three facies, approximate  $C_{org}$  budgets can be derived for each region and a net burial of  $3.5\ mmol\ C_{org}\ m^{-2}\ d^{-1}$  in the inner topset necessary to balance the initial river supply to the system can be obtained by difference (Figure 21). This latter estimated burial flux compares reasonably well with an estimate of  $7.3\ mmol\ C_{org}\ m^{-2}\ d^{-1}$  on the inner midtopset made from apparent sediment accumulation rates [Brunskill et al., 2007a].

[61] These diagenetic  $C_{org}$  cycle budgets have large uncertainties and are subject to substantial seasonal excursions, particularly in the inputs to the seabed and remineralization of labile marine  $C_{org}$  and macrodetritus (Figure 8) [Aller et al., 2008]. Nevertheless, they provide a sense of how the system operates in terms of processing sedimentary  $C_{org}$  as it cascades progressively through the clinoform facies to the foreset and bottomset depocenters. The inner and midtopset store ~13–27% of the initial river supply of terrestrial  $C_{org}$ , remineralize ~56%, and accumulate ~34% of the total sediment. In contrast, the outer topset and foreset (20–50 m) store ~23% of the river  $C_{org}$  flux, remineralize ~8.6% of the terrestrial  $C_{org}$ , and accumulate ~66% of the total detrital debris. These relative percentages, the  $\Sigma CO_2$  production rates, and the isotopic release patterns on the topset demonstrate that the topset region plays a far more critical role in the processing and remineralization of

terrestrial  $C_{org}$  than in storage (Figures 12, 15, 19, and 20). Net sediment accumulation is thus largely decoupled from remineralization patterns in the topset facies.

[62] The episodic refluxing of sedimentary debris and reexposure to oxygenated overlying water within and across the topset region promote suboxic diagenetic conditions in the reworked surface layer, exchange metabolites, and entrain reactive terrestrial and marine substrates (Figures 7 and 12) [Ogston et al., 2008; Aller et al., 2008]. These conditions optimize  $C_{org}$  decomposition as a result of oxygen exposure, the episodic resupply of Fe, Mn oxides as secondary oxidants, the removal of inhibitory metabolites, and the priming of refractory organic decomposition by the presence of labile substrates [Hedges et al., 1999; Keil et al., 2004; Aller, 1998; Aller and Blair, 2006]. The refluxing of particles vertically into the topset photic zone and horizontally across shelf onto periodically exposed tidal flats, must also enhance photochemical degradation processes [Mayer et al., 2006]. Consistent with this conceptual model, the sedimentary debris that eventually escapes the topset sedimentary incinerator is depleted in reactivity and in a substantial portion of its original terrestrial  $C_{org}$  load (Figures 6 and 20). The latter decreases from a range of  $\sim 0.5$ – $0.7\ mg\ C_{org}\ m^{-2}$  initially supplied by the rivers to  $\sim 0.19$ – $0.3\ mg\ C_{org}\ m^{-2}$  on the foreset and bottomset (calculated from the total  $C_{org}$  load of  $0.36$ – $0.42\ mg\ m^{-2}$ , Table 2, assuming  $-26.8$  and  $-20\ \text{‰}$  terrestrial and marine end-members).

[63] Therefore, despite receiving a high proportion of relatively old refractory material from a mountainous drainage area [Komada et al., 2004; Leithold et al., 2006], the diagenetic regime in the Gulf of Papua is effective at eliminating a large fraction of this input. Although not as efficient, as massive, or as energetic as the Amazon-Guianas region, which reduces initial terrestrial  $C_{org}$  loading to  $<0.12\ mg\ C\ m^{-2}$  over transport scales of  $\sim 600\ km$  [Aller and Blair, 2006], the Gulf of Papua deltaic topset system operates as a functionally similar sedimentary incinerator.

Residence time of sediment within this facies must be a primary determinant of remineralization and preservation of sedimentary C<sub>org</sub>.

## 7. Conclusions

[64] Terrestrial and marine C<sub>org</sub> having a wide spectrum of ages are remineralized throughout the deltaic complex, reflecting extensive cross-shelf particle exchange. As expected from boundary inputs, terrestrial C<sub>org</sub> dominates as a primary substrate at many sites inshore, and marine substrates dominate offshore.

[65] In general, diagenetic fractionation is the rule with average respiratory ΣCO<sub>2</sub> relatively young and heavy (e.g., labile marine) compared to bulk sedimentary C<sub>org</sub>, although all components are remineralized and terrestrial C<sub>org</sub> dominates when labile sources are locally available.

[66] The thin (~10–40 cm), physically reworked layer on the topset is a critical component of the delta diagenetic system, acting as a suboxic incinerator and eliminating >50% of the terrestrial C<sub>org</sub> in the initial river supply while storing only 13–27% as long-term accumulation. Sediment exported to the outer topset and foreset is depleted in reactive components.

[67] The net loss of sedimentary C<sub>org</sub> on the delta, while spatially variable, is dominated by the oxidation of terrestrial organic matter, including aged components >4000 years old, and its remineralization continues throughout the burial depth examined (7 m).

[68] Sediment refluxing and associated diagenetic conditions within the shallow delta topset zone are capable of efficiently incinerating the aged, refractory C<sub>org</sub> from the high-yield drainage basins characteristic of regions such as Oceania.

[69] **Acknowledgments.** Irena Zagorskis, John Pfitzner, Caterina Panzeca, Megan Dantzer, Vanessa Madrid, Lynn Abramson, Vasso (Bessy) Alexandratos, Christina Heilbrun, Steve Boyle, Miguel Goñi, Chuck Nittrouer, Josephine Aller, Catherine Thompson, Laurel Childress, and numerous additional participants and technical staff provided invaluable aid in the field and laboratory. The expertise and efforts of the Masters and crews of the R/V *Harry Messel*, R/V *Franklin*, and R/V *Cape Ferguson* from AIMS and R/V *Melville*, Scripps Institute of Oceanography were, of course, critical to the success of the project. We thank the reviewers for critical comments. NOSAMS analyses reflect facility support from NSF Cooperative Agreement OCE-9807266. Research support came from NSF Oceanography Program, grant OCE0219919.

## References

- Aalto, R., J. W. Lauer, and W. E. Dietrich (2008), Spatial and temporal dynamics of sediment accumulation and exchange along Strickland River floodplains (Papua New Guinea) over decadal-to-centennial timescales, *J. Geophys. Res.*, doi:10.1029/2006JF000627, in press.
- Aller, J. Y., and R. C. Aller (2004), Physical disturbance creates bacterial dominance of benthic biological communities in tropical deltaic environments of the Gulf of Papua, *Cont. Shelf Res.*, 24, 2395–2416.
- Aller, J. Y., D. M. Alongi, and R. C. Aller (2008), Biological indicators of seasonal sedimentary dynamics in the Gulf of Papua, *J. Geophys. Res.*, doi:10.1029/2006JF000823, in press.
- Aller, R. C. (1998), Mobile deltaic and continental shelf muds as fluidized bed reactors, *Mar. Chem.*, 61, 143–155.
- Aller, R. C., and N. E. Blair (1996), Sulfur diagenesis and burial on the Amazon Shelf: Major control by physical sedimentation processes, *Geo Mar. Lett.*, 16, 3–10.
- Aller, R. C., and N. E. Blair (2004), Early diagenetic remineralization of sedimentary organic C in the Gulf of Papua deltaic complex (Papua New Guinea): Net loss of terrestrial C and diagenetic fractionation of C isotopes, *Geochim. Cosmochim. Acta*, 68, 1815–1825.
- Aller, R. C., and N. E. Blair (2006), Carbon remineralization in the Amazon-Guianas tropical mobile mudbelt: A sedimentary incinerator, *Cont. Shelf Res.*, 26, 2241–2259.
- Aller, R. C., N. E. Blair, Q. Xia, and P. D. Rude (1996), Remineralization rates, recycling and storage of carbon in Amazon shelf sediments, *Cont. Shelf Res.*, 16, 753–786.
- Aller, R. C., A. Hannides, C. Heilbrun, and C. Panzeca (2004), Coupling of early diagenetic processes and sedimentary dynamics in tropical shelf environments: The Gulf of Papua deltaic complex, *Cont. Shelf Res.*, 24, 2455–2486.
- Alongi, D. M. (1991), The role of intertidal mudbanks in the diagenesis and export of dissolved and particulate materials from the Fly Delta, Papua New Guinea, *J. Explor. Mar. Biol. Ecol.*, 149, 81–107.
- Alongi, D. M. (1995), Decomposition and recycling of organic matter in muds of the Gulf of Papua, northern Coral Sea, *Cont. Shelf Res.*, 15, 1319–1337.
- Alongi, D. M. (1998), *Coastal Ecosystem Processes*, 419 pp., CRC Press, Boca Raton, Fla.
- Alongi, D. M., and A. I. Robertson (1995), Factors regulating benthic food chains in tropical river deltas and adjacent shelf areas, *Geo Mar. Lett.*, 15, 145–152.
- Alongi, D. M., P. Christoffersen, F. Tirindji, and A. I. Robertson (1992), The influence of freshwater and material export on sedimentary facies and benthic processes within the Fly Delta and adjacent Gulf of Papua (Papua New Guinea), *Cont. Shelf Res.*, 12, 287–326.
- Alongi, D. M., P. Christoffersen, and F. Tirindji (1993), The influence of forest type on microbial-nutrient relationships in tropical mangrove sediments, *J. Explor. Mar. Biol. Ecol.*, 171, 201–223.
- Benner, R. (2004), What happens to terrestrial organic matter in the ocean?, *Mar. Chem.*, 92, 307–310.
- Berner, R. A. (1980), *Early Diagenesis*, 241 pp., Princeton Univ. Press, Princeton, N. J.
- Berner, R. A. (1982), Burial of organic carbon and pyrite sulfur in the modern ocean: Its geochemical significance, *Am. J. Sci.*, 282, 451–473.
- Bird, M. I., S. G. Haberle, and A. R. Chivas (1994), Effect of altitude on the carbon isotope composition of forest and grassland soils from Papua New Guinea, *Global Biogeochem. Cycles*, 8, 13–22.
- Bird, M. I., G. J. Brunskill, and A. R. Chivas (1995), Carbon isotope composition of sediments from the Gulf of Papua, *Geo Mar. Lett.*, 15, 153–159.
- Blair, N. E., E. L. Leithold, S. T. Ford, K. A. Peeler, J. C. Holmes, and D. W. Perkey (2003), The persistence of memory: The fate of ancient sedimentary organic carbon in a modern sedimentary system, *Geochim. Cosmochim. Acta*, 67, 63–74.
- Blair, N. E., E. L. Leithold, and R. C. Aller (2004), From bedrock to burial: The evolution of particulate organic carbon across coupled watershed-continental margin systems, *Mar. Chem.*, 92, 141–156.
- Boudreau, B. P. (1997), *Diagenetic Models and Their Implementation*, 414 pp., Springer-Verlag, Berlin.
- Bouillon, S., F. Dahdouh-Guebas, A. Rao, N. Koedam, and F. Dehairs (2003), Sources of organic carbon in mangrove sediments: Variability and possible ecological implications, *Hydrobiologia*, 495, 33–39.
- Brunskill, G. J., K. J. Woolfe, and I. Zagorskis (1995), Distribution of riverine sediment chemistry on the shelf, slope and rise of the Gulf of Papua, *Geo Mar. Lett.*, 15, 160–165.
- Brunskill, G. J., D. M. Alongi, and K. J. Woolfe (1996), Terrestrial and marine sediments in the Gulf of Papua: Organic carbon, sulfur and iron relationships, in *Proceedings of the IOC-Westpac Third International Scientific Symposium, Bali, Indonesia*, pp. 429–438, Res. and Dev. Cent. for Oceanol., Indonesian Inst. of Sci., Jakarta.
- Brunskill, G. J., I. Zagorskis, and J. Pfitzner (2002), Carbon burial rates in sediments, and a carbon mass balance, of the Herbert River region of the Great Barrier Reef continental shelf, North Queensland, Australia, *Estuarine Coastal Shelf Sci.*, 54, 677–700.
- Brunskill, G. J., I. Zagorskis, and J. Pfitzner (2003), Geochemical mass balance for lithium, boron, and strontium in the Gulf of Papua, Papua New Guinea (Project TROPICS), *Geochim. Cosmochim. Acta*, 67, 3365–3383.
- Brunskill, G. J., I. Zagorskis, and J. Pfitzner (2007a), A mass balance for copper in the rivers, estuaries, shelf and slope of the Gulf of Papua, Papua New Guinea, in *The Fly River System, Papua New Guinea: A Natural History*, edited by B. Bolton, Elsevier, New York, in press.
- Brunskill, G. J., I. Zagorskis, and J. Pfitzner (2007b), C, N, P mass balance for tropical coastal seas of Australia and Papua New Guinea, in *Carbon and Nutrient Fluxes in Continental Margins: A Global Synthesis, Part IV: Tropical Margins, Int. Geosphere Biosphere Program Ser.*, edited by G. J. Brunskill, Springer-Verlag, Stuttgart, Germany, in press.
- Burdige, D. J. (2007), Preservation of organic matter in marine sediments: Controls, mechanisms, and an imbalance in sediment organic carbon budgets?, *Chem. Rev.*, 107, 467–485.

- Chanton, J. P., and C. S. Martens (1988), Seasonal variations in ebullitive flux and carbon isotopic composition of methane in a tidal freshwater estuary, *Global Biogeochem. Cycles*, 2, 289–298.
- Cifuentes, L. A., R. B. Coffin, L. Solorzano, W. Cardenas, J. Espinoza, and R. R. Twilley (1996), Isotopic and elemental variations of carbon and nitrogen in a mangrove estuary, *Estuarine Coastal Shelf Sci.*, 43, 781–800.
- Dalrymple, R. W., E. A. Baker, P. T. Harris, and M. G. Hughes (2003), Sedimentology and stratigraphy of a tide-dominated foreland-basin delta (Fly River, Papua New Guinea), in *Tropical Deltas of Southeast Asia and Vicinity: Sedimentology, Stratigraphy, and Petroleum Geology*, edited by F. H. Sidi et al., *Spec. Publ. SEPM Soc. Sediment. Geol.*, 76, 147–173.
- Druffel, E. R. M., S. Griffin, T. P. Guilderson, M. Kahngarian, J. Southon, and D. P. Schrag (2001), Changes of subtropical North Pacific radiocarbon and correlation with climate variability, *Radiocarbon*, 43, 15–25.
- Druffel, E. R. M., J. E. Bauer, and S. Griffin (2005), Input of particulate organic and dissolved inorganic carbon from the Amazon to the Atlantic Ocean, *Geochem. Geophys. Geosyst.*, 6, Q03009, doi:10.1029/2004GC000842.
- Goñi, M. A., M. B. Yunker, R. W. Macdonald, and T. I. Eglinton (2005), The supply and preservation of ancient and modern components of organic carbon in the Canadian Beaufort Shelf of the Arctic Ocean, *Mar. Chem.*, 93, 53–73.
- Goñi, M. A., N. Monacci, R. Gisewhite, A. Ogston, J. Crockett, and C. Nittrouer (2006), Distribution and sources of particulate organic matter in the water column and sediments of the Fly River Delta, Gulf of Papua (Papua New Guinea), *Estuarine Coastal Shelf Sci.*, 69, 225–245.
- Goñi, M. A., N. Monacci, R. Gisewhite, J. Crockett, C. Nittrouer, A. Ogston, S. R. Alin, and R. Aalto (2008), Terrigenous organic matter in sediments from the Fly River Delta (Papua New Guinea), *J. Geophys. Res.*, doi:10.1029/2006F000653, in press.
- Goto, K., T. Komatsu, and T. Furukawa (1962), Rapid colorimetric determination of manganese in waters containing iron, *Anal. Chim. Acta*, 27, 331–334.
- Hall, P. O. J., and R. C. Aller (1992), Rapid, small-volume, flow injection analysis for  $\Sigma\text{CO}_2$  and  $\text{NH}_4^+$  in marine and freshwaters, *Limnol. Oceanogr.*, 37, 1113–1119.
- Harris, P. T., E. K. Baker, A. R. Cole, and S. A. Short (1993), A preliminary study of sedimentation in the tidally dominated Fly River Delta, Gulf of Papua, *Cont. Shelf Res.*, 13, 441–472.
- Harris, P. T., C. B. Pattiariatchi, J. B. Keene, R. W. Dalrymple, J. V. Gardner, E. K. Baker, A. R. Cole, D. Mitchell, P. Gibbs, and W. W. Schroeder (1996), Late Quaternary deltaic and carbonate sedimentation in the Gulf of Papua foreland basin: Response to sea-level change, *J. Sediment. Res.*, 66, 801–819.
- Harris, P. T., M. G. Hughes, E. K. Baker, R. W. Dalrymple, and J. B. Keene (2004), Sediment transport in distributary channels and its export to the pro-deltaic environment in a tidally dominated delta: Fly River, Papua New Guinea, *Cont. Shelf Res.*, 24, 2431–2454.
- Hedges, J. I., and R. G. Keil (1995), Sedimentary organic matter preservation: An assessment and speculative synthesis, *Mar. Chem.*, 49, 81–115.
- Hedges, J. I., F. S. Hu, A. H. Devol, H. E. Hartnett, E. Tsamakis, and R. G. Keil (1999), Sedimentary organic matter preservation: A test for selective degradation under oxic conditions, *Am. J. Sci.*, 299, 529–555.
- Jennerjahn, T. C., and V. Ittekot (2002), Relevance of mangroves for the production and deposition of organic matter along tropical continental margins, *Naturwissenschaften*, 89, 23–30.
- Keil, R. G., L. M. Mayer, P. D. Quay, J. E. Richey, and J. I. Hedges (1997), Loss of organic matter from riverine particles in deltas, *Geochim. Cosmochim. Acta*, 61, 1507–1512.
- Keil, R. G., A. F. Dickens, T. Arnarson, B. L. Nunn, and A. H. Devol (2004), What is the oxygen exposure time of laterally transported organic matter along the Washington margin?, *Mar. Chem.*, 92, 157–165.
- Komada, T., E. R. M. Druffel, and S. E. Trumbore (2004), Oceanic export of relict carbon by small mountainous rivers, *Geophys. Res. Lett.*, 31, L07504, doi:10.1029/2004GL019512.
- Kuehl, S. A., C. A. Nittrouer, D. J. DeMaster, and T. B. Curtin (1985), A long square-barrel gravity corer for sedimentological and geochemical investigation of fine-grained sediments, *Mar. Geol.*, 62, 365–370.
- Leithold, E. L., N. E. Blair, and D. W. Perkey (2006), Geomorphologic controls on the age of particulate organic carbon from small mountainous and upland rivers, *Global Biogeochem. Cycles*, 20, GB3022, doi:10.1029/2005GB002677.
- Ludwig, W., J. L. Probst, and S. Kempe (1996), Predicting the oceanic input of organic carbon by continental erosion, *Global Biogeochem. Cycles*, 10, 23–41.
- Lyons, W. B., C. A. Nezat, A. Carey, and D. M. Hicks (2002), Organic carbon fluxes to the ocean from high-standing islands, *Geology*, 30, 443–446.
- Martin, W. R., A. P. McNichol, and D. C. McCorkle (2000), The radiocarbon age of calcite dissolving at the sea floor: Estimates from pore water data, *Geochim. Cosmochim. Acta*, 64, 1391–1404.
- Martin, D. P., C. A. Nittrouer, A. S. Ogston, and J. S. Crockett (2008), Tidal and seasonal dynamics of a muddy inner shelf environment, Gulf of Papua, *J. Geophys. Res.*, doi:10.1029/2006JF000681, in press.
- Mayer, L. M. (1994a), Surface area control of organic carbon accumulation in continental shelf sediments, *Geochim. Cosmochim. Acta*, 58, 1271–1284.
- Mayer, L. M. (1994b), Relationships between mineral surfaces and organic carbon concentrations in soils and sediments, *Chem. Geol.*, 114, 347–363.
- Mayer, L. M., L. L. Schick, K. Skorko, and E. Boss (2006), Photodissolution of particulate organic matter from sediments, *Limnol. Oceanogr.*, 51, 1064–1071.
- McAlpine, J. R., G. Keig, and R. Falls (1983), *Climate of Papua New Guinea*, Aust. Natl. Univ. Press, Canberra.
- McCallister, S. L., J. E. Bauer, J. Cherrier, and H. W. Ducklow (2004), Assessing sources and ages of organic matter supporting river and estuarine bacterial production: A multiple-isotope ( $\Delta^{14}\text{C}$ ,  $\delta^{13}\text{C}$ ,  $\delta^{15}\text{N}$ ) approach, *Limnol. Oceanogr.*, 49, 1687–1702.
- McKee, B. A., R. C. Aller, M. A. Allison, T. A. Bianchi, and G. C. Kineke (2004), Transport and transformation of dissolved and particulate materials on continental margins influenced by major rivers: Benthic boundary layer and seabed processes, *Cont. Shelf Res.*, 24, 899–926.
- McKinnon, A. D., J. H. Carleton, and S. Duggan (2007), Pelagic production and respiration in the Gulf of Papua during May 2004, *Cont. Shelf Res.*, 27, 1643–1655.
- Meybeck, M. (1993), C, N, P and S in rivers: From sources to global inputs, in *Interactions of C, N, P and S: Biogeochemical Cycles and Global Change*, edited by R. Wollast, R. T. Mackenzie, and L. Cou, pp. 163–193, Springer, Berlin.
- Milliman, J. D. (1995), Sediment discharge to the ocean from small mountainous rivers: The New Guinea example, *Geo Mar. Lett.*, 15, 127–133.
- Milliman, J. D., and R. H. Meade (1983), World-wide delivery of river sediment to the oceans, *J. Geol.*, 91, 1–21.
- Milliman, J. D., and J. P. M. Syvitski (1992), Geomorphic/tectonic control of sediment discharge to the ocean: The importance of small mountainous rivers, *J. Geol.*, 100, 525–544.
- Milliman, J. D., K. L. Farnsworth, and C. S. Albertin (1999), Flux and fate of fluvial sediments leaving large islands in the East Indies, *J. Sea Res.*, 41, 97–107.
- Mitchell, A. (1982), Oceanographic observations in the Gulf of Papua and Torres Strait, 1979, *Data Rep. AIMS-OS-82-1*, Aust. Inst. of Mar. Sci., Townsville, Queensland.
- Moi, A. S. (2001), Rainfall, river level and SOI indices and navigation on the Fly River, paper presented at Annual Meeting, Aust. Mar. Sci. Assoc., Townsville, Queensland.
- Muhammad, Z., S. J. Bentley, L. A. Febo, A. W. Droxler, G. R. Dickens, L. C. Peterson, and B. N. Opdyke (2008), Excess  $^{210}\text{Pb}$  inventories and fluxes along the continental slope and basins of the Gulf of Papua, *J. Geophys. Res.*, doi:10.1029/2006JF000676, in press.
- Ogston, A. S., R. W. Sternberg, C. A. Nittrouer, D. P. Martin, M. A. Goñi, and J. S. Crockett (2008), Sediment delivery from the Fly River tidally dominated delta to the nearshore marine environment and the impact of El Niño, *J. Geophys. Res.*, doi:10.1029/2006JF000669, in press.
- Olsson, I. U. (1970), The use of oxalic acid as a standard, in *Radiocarbon Variations and Absolute Chronology, 12th Proceedings of the Nobel Symposium*, edited by I. U. Olsson, p. 37, John Wiley, Hoboken, N. J.
- Pickup, G., and V. H. Chewings (1983), The hydrology of the Purari and its environmental implications, in *The Purari: Tropical Environment of a High Rainfall River Basin*, edited by T. Petr, pp. 123–140, Dr. Junk, The Hague.
- Raymond, M. B. (1999), Geochemistry of small mountainous rivers of Papua New Guinea: local observations and global implications, M.S. thesis, 56 pp., Coll. of William and Mary, Williamsburg, Va.
- Raymond, P. A., and J. E. Bauer (2001), Use of  $^{14}\text{C}$  and  $^{13}\text{C}$  natural abundances for evaluating riverine, estuarine and coastal DOC and POC sources and cycling: A review and synthesis, *Org. Geochem.*, 32, 469–485.
- Robertson, A. I., and D. M. Alongi (1995), Role of riverine mangrove forests in organic carbon export to the tropical coastal ocean: A preliminary mass balance for the Fly Delta (Papua New Guinea), *Geo Mar. Lett.*, 15, 134–139.
- Robertson, A. I., P. Dixon, and D. M. Alongi (1998), The influence of fluvial discharge on pelagic production in the Gulf of Papua, northern Coral Sea, *Estuarine Coastal Shelf Sci.*, 46, 319–331.
- Salomons, W., and A. M. Eagle (1990), Hydrology, sedimentology and the fate and distribution of copper in mine-related discharges in the Fly river system, Papua New Guinea, *Sci. Total Environ.*, 97/98, 315–334.

- Sayles, F. L., and W. B. Curry (1988),  $\delta^{13}\text{C}$ , TCO<sub>2</sub>, and the metabolism of organic carbon in deep sea sediments, *Geochim. Cosmochim. Acta*, **45**, 1061–1086.
- Schlünz, B., and R. R. Schneider (2000), Transport of terrestrial organic carbon to the ocean by rivers: Re-estimating flux- and burial rates, *Int. J. Earth Sci.*, **88**, 599–606.
- Sivan, O., B. Lazar, Y. Yechiel, E. Boaretto, J. Heinemeier, and B. Herut (2002),  $^{14}\text{C}$  excess in deep-sea sediments porewater driven by diffusion: Southeast Mediterranean, *Limnol. Oceanogr.*, **47**, 565–570.
- Stookey, L. (1970), Ferrozine—New spectrophotometric reagent for iron, *Anal. Chem.*, **42**, 779–781.
- Stuiver, M., and H. A. Polach (1977), Reporting of  $^{14}\text{C}$  data, *Radiocarbon*, **19**, 355–363.
- Thom, B. G., and L. D. Wright (1983), Geomorphology of the Purari Delta, in *The Purari: Tropical Environment of a High Rainfall River Basin*, edited by T. Petr, pp. 47–65, Dr. Junk, The Hague.
- Toth, D. J., and A. Lerman (1977), Organic matter reactivity and sedimentation rates in the ocean, *Am. J. Sci.*, **277**, 265–285.
- Tromp, T. K., P. Van Cappellen, and R. M. Key (1995), A global model for the early diagenesis of organic carbon and organic phosphorus in marine sediments, *Geochim. Cosmochim. Acta*, **59**, 1259–1284.
- Trumbore, S. E., and S. H. Zheng (1996), Comparison of fractionation methods of soil organic matter C-14 analysis, *Radiocarbon*, **38**, 219–229.
- Viollier, E., P. W. Inglett, K. Hunter, A. N. Roychoudhury, and P. Van Cappellen (2000), The ferrozine method revisited: Fe(II)/Fe(III) determination in natural waters, *Appl. Geochem.*, **15**, 785–790.
- Walsh, J. P., and C. A. Nittrouer (2003), Contrasting styles of off-shelf sediment accumulation in New Guinea, *Mar. Geol.*, **196**, 105–125.
- Walsh, J. P., and C. A. Nittrouer (2004), Mangrove-bank sedimentation in a mesotidal environment with large sediment supply, Gulf of Papua, *Mar. Geol.*, **208**, 225–248.
- Walsh, J. P., C. A. Nittrouer, C. M. Palinkas, A. S. Ogston, R. W. Sternberg, and G. J. Brunskill (2004), Cliniform mechanics in the Gulf of Papua, New Guinea, *Cont. Shelf Res.*, **24**, 2487–2510.
- Wolanski, E., and M. Eagle (1991), Oceanography and sediment transport, Fly River estuary and Gulf of Papua, in *Proceedings, 10th Australasian Conference on Coastal and Ocean Engineering*, Publ. 21, pp. 453–457, Water Quality Cent., Auckland.
- Wolanski, E., G. L. Pickard, and D. L. B. Jupp (1984), River plumes, coral reefs and mixing in the Gulf of Papua and the northern Great Barrier Reef, *Estuarine Coastal Shelf Sci.*, **18**, 291–314.
- Wolanski, E., A. Norro, and B. King (1995), Water circulation in the Gulf of Papua, *Cont. Shelf Res.*, **15**, 185–212.

---

R. C. Aller, School of Marine and Atmospheric Sciences, State University of New York at Stony Brook, Stony Brook, NY 11794-5000, USA. (raller@notes.cc.sunysb.edu)

N. E. Blair, Department of Civil and Environmental Engineering, Department of Earth and Planetary Sciences, Northwestern University, Evanston, IL 60208, USA.

G. J. Brunskill, Australian Institute of Marine Science, PMB 3, Townsville, Qld 4810, Australia.